ISTANBUL TECHNICAL UNIVERSITY ★ GRADUATE SCHOOL

PREPARATION AND CHARACTERIZATION OF POLYACRYLONITRILE-BASED QUASI-SOLID-STATE ELECTROLYTES FOR LITHIUM-ION BATTERY APPLICATIONS

M.Sc. THESIS

Sabiha Ezgi KAYA

Department of Energy Science and Technology

Energy Science and Technology Programme

JANUARY 2024

ISTANBUL TECHNICAL UNIVERSITY ★ GRADUATE SCHOOL

PREPARATION AND CHARACTERIZATION OF POLYACRYLONITRILE-BASED QUASI-SOLID-STATE ELECTROLYTES FOR LITHIUM-ION BATTERY APPLICATIONS

M.Sc. THESIS

Sabiha Ezgi KAYA
(301191063)

Department of Energy Science and Technology

Energy Science and Technology Program

Thesis Advisor: Prof. Dr. Nilgün KARATEPE YAVUZ

JANUARY 2024

İSTANBUL TEKNİK ÜNİVERSİTESİ ★ LİSANSÜSTÜ EĞİTİM ENSTİTÜSÜ

LİTYUM-İYON PİL UYGULAMALARI İÇİN POLİAKRİLONİTRİL BAZLI YARI KATI HAL ELEKTROLİTLERİN HAZIRLANMASI VE KARAKTERİZASYONU

YÜKSEK LİSANS TEZİ

Sabiha Ezgi KAYA
(301191063)

Enerji Bilim ve Teknoloji Anabilim Dalı

Enerji Bilim ve Teknoloji Programı

Tez Danışmanı: Prof. Dr. Nilgün KARATEPE YAVUZ

OCAK 2024

Sabiha Ezgi KAYA, a M.Sc. student of ITU Graduate School student ID 301191063, successfully defended the thesis entitled "PREPARATION AND CHARACTERIZATION OF POLYACRYLONITRILE-BASED QUASI-SOLID-STATE ELECTROLYTES FOR LITHIUM-ION BATTERY APPLICATIONS", which she prepared after fulfilling the requirements specified in the associated legislations, before the jury whose signatures are below.

Thesis Advisor :	**Prof. Dr. Nilgün KARATEPE YAVUZ** Istanbul Technical University	.....
Jury Members :	**Prof. Dr. Üner ÇOLAK** Istanbul Technical University	.....
	Assoc. Prof. Dr. Metin GENÇTEN Yıldız Technical University	.....

Date of Submission : 5 January 2024
Date of Defense : 22 January 2024

To my family,

FOREWORD

Foremost, I express my endless gratitude to my advisor Prof. Dr. Nilgün KARATEPE YAVUZ for her guidance, kindness and invaluable motivation throughout this thesis study.

I am indebted to Dr. Ömer EROĞLU for sharing his knowledge and criticism at all stages of the work. I am thankful to Ph.D. candidate Selin DEMİRCİ for her support and help in the technical analyses. I also would like to thank Res. Asst. Ph.D. candidate Gökçen GÖKÇELİ KAHVECİ for her help, especially with the TG/DSC analysis.

Moreover, I owe Prof. Dr. Fatma Seniha GÜNER a debt of gratitude for her help with material supply.

I am also grateful to Prof. Dr. Bahire Filiz ŞENKAL and Prof. Dr. Ahmet SİRKECİOĞLU for their help with the FTIR analysis.

Lastly, I would like to emphasize that this study could not have been completed without the patience and emotional support of my beloved family.

January 2024

Sabiha Ezgi KAYA
(Chemical Engineer)

TABLE OF CONTENTS

Page

FOREWORD ..... **ix**
TABLE OF CONTENTS ..... **xi**
ABBREVIATIONS ..... **xiii**
SYMBOLS ..... **xv**
LIST OF TABLES ..... **xvii**
LIST OF FIGURES ..... **xix**
SUMMARY ..... **xxi**
ÖZET ..... **xxiii**
1. INTRODUCTION **1**
2. LITERATURE REVIEW **5**
2.1 Overview of Batteries 5
2.1.1 Rechargeable batteries 6
2.1.2 Lithium-ion batteries 8
2.1.2.1 Cathode materials for li-ion batteries 8
2.1.2.2 Anode materials for li-ion batteries 9
2.1.2.3 Electrolyte of li-ion batteries 10
2.2 Solid-State Electrolytes for Li-Ion Batteries 11
2.2.1 Ceramic-based (inorganic) solid-state electrolytes 11
2.2.2 Polymer-based (organic) solid-state electrolytes 14
2.2.3 Polymer/ceramic composite solid-state electrolytes 16
2.3 Gel Polymer Electrolytes 19
3. EXPERIMENTAL STUDY **23**
3.1 Materials 23
3.1.1 Polyacrylonitrile 23
3.1.2 Polyethylene glycol 23
3.1.3 Dimethylformamide 24
3.1.4 Silicon dioxide 24
3.1.5 $LiPF_6$ in EC/DEC/DMC 25
3.2 Preparation of Gel Polymer Electrolytes 25
3.3 Characterization of the Electrolyte Samples 26
3.3.1 Fourier transform infrared spectroscopy 26
3.3.2 Thermogravimetry and differential scanning calorimetry 27
3.3.3 Electrochemical measurements 28
3.3.3.1 Ionic conductivity 28
3.3.3.2 Cation transference number 29
3.3.3.3 Electrochemical stability window 30
3.3.3.4 Half-cell performance 31
4. RESULTS AND DISCUSSION **33**
4.1 Results for the Gel Polymer Electrolytes 33
4.1.1 FTIR analysis of the gel polymer electrolytes 33
4.1.2 TG and DSC analysis of the gel polymer electrolytes 36

4.1.3 Ionic conductivity analysis of the gel polymer electrolytes 41
4.1.4 Li-ion transference number analysis of the gel polymer electrolytes 42
4.1.5 Electrochemical stability analysis of the gel polymer electrolytes 43
4.2 Results for the Composite Gel Polymer Electrolytes 45
4.2.1 FTIR analysis of the composite gel polymer electrolytes 45
4.2.2 TG and DSC analysis of the composite gel polymer electrolytes 48
4.2.3 Ionic conductivity analysis of the composite gel polymer electrolytes 53
4.2.4 Li-ion transference number analysis of the composite gel polymer electrolytes 54
4.2.5 Electrochemical stability analysis of the composite gel polymer electrolytes 55
4.2.6 Half-cell performance analysis of the composite gel polymer electrolytes 57
5. CONCLUSIONS AND RECOMMENDATIONS 59
REFERENCES 61
CURRICULUM VITAE 69

ABBREVIATIONS

AC : Alternative Current
CB : Carbon Black
DC : Direct Current
DEC : Diethyl Carbonate
DMC : Dimethyl Carbonate
DMF : N,N-Dimethylformamide
DSC : Differential Scanning Calorimetry
EC : Ethylene Carbonate
EIS : Electrochemical Impedance Spectroscopy
ESW : Electrochemical Stability Window
EV : Electric Vehicle
FTIR : Fourier Transform Infrared Spectroscopy
HEV : Hybrid Electric Vehicle
LSV : Linear Sweep Voltammetry
NMP : N-Methyl-2-Pyrrolidone
PAN : Polyacrylonitrile
PC : Propylene Carbonate
PEG : Polyethylene Glycol
PVDF : Poly(vinylidene fluoride)
SEI : Solid-Electrolyte Interface
SSE : Solid-State Electrolyte
TG : Thermogravimetry

SYMBOLS

A	**:** Surface area
C	**:** Capacity
I_0	**:** Initial current
I_{ss}	**:** Steady-state current
l	**:** Thickness
M_w	**:** Molecular weight
Q_{peak}	**:** Heat flow of exothermic peak
$R_{i,0}$	**:** Initial interfacial resistance
R_b	**:** Bulk resistance
$R_{i,ss}$	**:** Steady-state interfacial resistance
t_+	**:** Cationic transference number
T_d	**:** Decomposition temperature
T_g	**:** Glass-transition temperature
T_{peak}	**:** Temperature of exothermic peak
W_f	**:** Final residual weight
Z	**:** Impedance
Z'	**:** Resistive impedance element
Z"	**:** Capacitive impedance element
ΔV	**:** Step voltage
σ	**:** Ionic conductivity

LIST OF TABLES

Page

Table 2.1 : Certain characteristics of the main rechargeable batteries [15]. **7**
Table 2.2 : The advantages and disadvantages of liquid, solid polymer and gel polymer electrolytes [43, 44]. **20**
Table 3.1 : Compositions of the casting solutions for the gel polymer electrolytes. **25**
Table 3.2 : Compositions of the casting solutions for the composite gel polymer electrolytes. **26**
Table 4.1 : Wavenumbers correspond to vibrational modes for PAN and PEG based on literature data. **33**
Table 4.2 : T_d and W_f values for the polymer samples with varying compositions of PAN and PEG..... **38**
Table 4.3 : T_{peak}, Q_{peak} and T_g values for the polymer samples with varying compositions of PAN and PEG. **40**
Table 4.4 : Calculation of the ionic conductivity of the polymer electrolyte samples PAN, S1, S2, S3 and S4. ..... **41**
Table 4.5 : The interfacial resistance, current and lithium-ion transference number of the polymer electrolyte samples PAN, S1, S2, S3 and S4. ..... **43**
Table 4.6 : Electrochemical stability window of the polymer electrolyte samples PAN, S1, S2, S3 and S4. ..... **45**
Table 4.7 : T_d and W_f values for the composite polymer samples with varying compositions of PAN, PEG and SiO_2. ..... **50**
Table 4.8 : T_{peak}, Q_{peak} and T_g values for the composite polymer samples with varying compositions of PAN, PEG and SiO_2. ..... **53**
Table 4.9 : Calculation of the ionic conductivity of the composite gel polymer electrolytes. **54**
Table 4.10 : Calculation of the lithium-ion transference number of the composite gel polymer electrolytes C1, C2, C3 and C4..... **55**
Table 4.11 : Electrochemical stability window of the composite gel polymer electrolytes C1, C2, C3 and C4. ..... **56**

LIST OF FIGURES

Page

Figure 1.1 : Global demand for li-ion batteries over the next decade [5]. **2**
Figure 1.2 : A number of next generation cathode materials modelled with the conventional anodes and lithium-metal anode [9]. **3**
Figure 2.1 : Components and working mechanism of a lithium-ion cell [11]. **5**
Figure 2.2 : Crystal structures of layered $LiMO_2$ (M= Mn, Co and Ni), spinel $LiMn_2O_4$ and olivine $LiFePO_4$ [6]..... **8**
Figure 2.3 : Li^+ ion transport a) in grain boundaries, b) within grains and c) between grains [31]. **12**
Figure 3.1 : The chemical structure of PAN polymer matrix [47]..... **24**
Figure 3.2 : The unit structure of a PEG molecule [50]..... **24**
Figure 3.3 : The chemical structure of silicon dioxide [54]..... **24**
Figure 3.4 : A typical mid-IR transmission spectrum [63]. **27**
Figure 3.5 : Ionic conductivity measurement. a) Cell configuration with solid electrolyte and blocking electrodes. b) Equivalent circuit representation. c) Nyquist plot of the equivalent circuit for ideal systems and the change for real systems [65]. **29**
Figure 4.1 : FTIR spectra of the dry polymer samples PAN, PEG, S1, S2, S3 and S4. ..... **34**
Figure 4.2 : FTIR spectra of the polymer electrolytes PAN, S1, S2, S3 and S4. ..... **35**
Figure 4.3 : TG curves of a) dry polymer samples and b) polymer electrolyte samples for PAN, S1, S2, S3 and S4..... **37**
Figure 4.4 : DSC curves for dry polymer samples of PAN, S1, S2, S3 and S4..... **38**
Figure 4.5 : DSC curves for polymer electrolyte samples of PAN, S1, S2, S3 and S4. ..... **39**
Figure 4.6 : The first derivatives of the DSC curves for dry polymer samples of PAN, S1, S2, S3 and S4 in the range of 40-120 °C. **39**
Figure 4.7 : The first derivatives of the DSC curves for polymer electrolyte samples of PAN, S1, S2, S3 and S4 in the range of 40-120 °C. **40**
Figure 4.8 : AC impedance spectroscopy of the polymer electrolyte samples. **41**
Figure 4.9 : Chronoamperometry curves by 10 mV DC polarization with inset AC EIS plots of the polymer electrolyte samples: a) PAN, b) S1, c) S2, d) S3 and e) S4. ..... **42**
Figure 4.10 : LSV plots of the polymer electrolyte samples: a) PAN, b) S1, c) S2, d) S3 and e) S4..... **44**
Figure 4.11 : FTIR spectra for the samples with PAN/PEG=2:1 (w/w): a) C1 and dry C1, and b) C2 and dry C2..... **46**
Figure 4.12 : FTIR spectra of the gel polymer electrolytes with different SiO_2 weight ratios for PAN/PEG=2:1 (w/w). **46**
Figure 4.13 : FTIR spectra for the samples with PAN/PEG=1:1 (w/w): a) C3 and dry C3, and b) C4 and dry C4..... **47**

Figure 4.14 : FTIR spectra of the gel polymer electrolytes with different SiO_2 weight ratios for PAN/PEG=1:1 (w/w). **48**
Figure 4.15 : TG curves of a) dry composite polymer samples and b) composite polymer electrolyte samples for C1, C2, C3 and C4. ..... **49**
Figure 4.16 : DSC curves of a) dry composite polymer samples and b) composite polymer electrolyte samples for C1, C2, C3 and C4. ..... **51**
Figure 4.17 : The first derivatives of the DSC curves of a) dry composite polymer samples and b) composite polymer electrolyte samples for C1, C2, C3 and C4 in the range of 40-200 °C. **52**
Figure 4.18 : AC impedance spectroscopy of the composite gel polymer electrolytes. **53**
Figure 4.19 : Chronoamperometry curves by 10 mV DC polarization with inset AC EIS plots of the composite gel polymer electrolytes: a) C1 and b) C2. .. **54**
Figure 4.20 : Chronoamperometry curves by 10 mV DC polarization with inset AC EIS plots of the composite gel polymer electrolytes: a) C3 and b) C4. .. **55**
Figure 4.21 : LSV plots of the composite gel polymer electrolytes: a) C1, b) C2, c) C3 and d) C4. ..... **56**
Figure 4.22 : Galvanostatic charge and discharge profile for the first cycle of the half-cells with the electrolyte samples: a) C2 and b) C4. ..... **57**

PREPARATION AND CHARACTERIZATION OF POLYACRYLONITRILE-BASED QUASI-SOLID-STATE ELECTROLYTES FOR LITHIUM-ION BATTERY APPLICATIONS

SUMMARY

The use of lithium-ion battery in various energy storage applications, e.g. portable electronic devices, electric vehicles and power grids, has made the safety matter one of its key features to consider. The conventional liquid electrolytes of the lithium-ion batteries pose a number of hazards such as leakage, fire, explosion, etc. In this regard, solid-state and quasi-solid-state electrolytes provide an alternative approach as they partially or fully eliminate the organic solvent usage in the battery. Particularly, gel electrolytes are considered as the transition stage between the conventional liquid and all-solid-state electrolytes.

In the study, gel polymer and composite gel polymer electrolytes with different compositions were prepared via the solution casting method and following immersion in the liquid electrolyte. The polymer host polyacrylonitrile (PAN) and the plasticizer polyethylene glycol (PEG) are the main components in common while the filler material silicon dioxide (SiO_2) is only found in the composite gel electrolytes. Lithium hexafluorophosphate solution in organic solvent mixture of ethylene carbonate, diethyl carbonate and dimethyl carbonate (1M $LiPF_6$ in EC/DEC/DMC=1:1:1 (v/v/v)) was used as the liquid electrolyte. The prepared electrolytes were structurally and thermally characterized by the Fourier transform infrared spectroscopy method and thermogravimetry/differential scanning calorimetry analysis, respectively.

First of all, the room temperature ionic conductivity was estimated via electrochemical impedance spectroscopy (EIS), and the highest value of 5.56×10^{-3} S/cm was measured for a gel polymer electrolyte while the value of 7.00×10^{-3} S/cm was obtained for a composite gel polymer electrolyte. Moreover, the highest Li^+ ion transference number among all the electrolytes was calculated as 0.89 through EIS and chronoamperometry techniques. Furthermore, electrochemical stabilities of the electrolytes were determined by applying linear sweep voltammetry method. One of the gel polymer electrolytes exhibited oxidative stability reaching above 4.5 V, and two of the composite gel polymer electrolytes showed oxidative stability exceeding 5 V. Lastly, these two composite gel polymer electrolytes were used in the half-cell design, and the initial galvanostatic charge-discharge cycle performance of those cells were evaluated and compared.

In conclusion, the gel and composite gel polymers, that were prepared, characterized and subjected to a number of electrochemical battery tests within the scope of the study, were assessed as the potential candidates to be used in the future lithium-ion battery studies. Further studies on this topic would be on multiple charge-discharge cycle tests and on increasing the discharge capacity.

LİTYUM-İYON PİL UYGULAMALARI İÇİN POLİAKRİLONİTRİL BAZLI YARI KATI HAL ELEKTROLİTLERİN HAZIRLANMASI VE KARAKTERİZASYONU

ÖZET

Lityum-iyon pilin taşınabilir elektronik cihaz, elektrikli araç, şebeke ölçeğinde enerji depolama gibi çeşitli uygulamalarda kullanılması, güvenlik konusunu göz önünde bulundurulması gereken temel özelliklerinden biri yapmıştır. Güncel olarak lityum-iyon pillerde kullanılmakta olan sıvı elektrolitler ile bunların içeriklerindeki organik çözücüler sızıntı, yanma, patlama gibi bazı tehlikeleri oluşturmaktadır. Bunun yanı sıra, 2030 yılı itibariyle toplam lityum-iyon pil talebinin yaklaşık olarak 4,700 GWh olması ve bu talebin büyük bir kısmının ait olacağı elektrikli araçların pil başına 500 Wh/kg'dan fazla enerji yoğunluğuna sahip olması öngörülmektedir. Enerji yoğunluğunu arttırmayı sağlamanın başlıca yollarından biri pil yapısında yüksek kapasiteli katot malzemelerini uygulamaktır. Ancak, bu alternatif pil tasarımları yine sıvı elektrolitlerle ilişkilendirilebilecek şekilde kısa devre, termal kaçak, aşırı ısınma gibi olası problemlere yol açmaktadır. Tüm bu durumlar değerlendirildiğinde, elektrolit konusuna farklı bir bakış açısıyla yaklaşmak gerektiği anlaşılmıştır.

Bu bağlamda, katı ve yarı katı haldeki elektrolitler, pil içeriğinde organik çözücü kullanımını tamamen ya da kısmen ortadan kaldırdıkları için, alternatif yaklaşım olarak ön plana çıkmaktadırlar. Özellikle jel formdaki elektrolitler, geleneksel sıvı elektrolitli pillerden tamamen katı haldeki pillere bir geçiş aşaması olarak yorumlanmaktadır. Yüksek güvenliğe sahip olmasına karşın, düşük iyonik iletkenlik başta olmak üzere görece zayıf performans özellikleri sergileyen katı polimer elektrolitler yerine, işlenebilirliği daha kolay olan jel polimer elektrolitler lityum-iyon pil konusunda son dönemde üzerine çalışmalar yapılan bir alt başlık olmuştur. İçeriğine plastikleştirici madde eklenen katı polimer malzemeler jel yapıya dönüşerek daha yüksek iyonik iletkenlik göstermekte olup, yine söz konusu bu plastikleştirici maddelerin neden olduğu mekanik kararsızlık çeşitli inorganik seramik dolgu malzemeleri kullanılarak kompanse edilebilmektedir. Bu türdeki elektrolit modeller kompozit jel polimer elektrolit olarak literatürde yer almaktadır.

Bu tez çalışmasında, değişen oranlı bileşenlerden oluşan jel ve kompozit jel polimer yapıdaki elektrolitler, çözelti döküm tekniği ile elde edilen polimer filmlerin sıvı elektrolitte belirli bir süre boyunca bekletilmesi yöntemiyle hazırlanmıştır. Polimer malzeme olarak poliakrilonitril (PAN) ve plastikleştirici malzeme olarak polietilen glikol (PEG) jel ve kompozit jel elektrolitlerde kullanılan ortak bileşenler olup, kompozit jel polimer elektrolitlerde ek olarak silikon dioksit (SiO_2) dolgu malzemesi kullanılmıştır. Eşit hacimli etilen karbonat, dietil karbonat ve dimetil karbonat organik çözücü karışımında çözünmüş lityum hekzaflorofosfat tuz çözeltisi (1M $LiPF_6$-EC/DEC/DMC (hacimce 1:1:1)) çalışmada sıvı elektrolit olarak kullanılmıştır. Deneysel çalışmanın tamamı birbirini izleyen iki ana alt çalışma olarak gerçekleştirilmiştir. İlk çalışmada jel polimer elektrolitlerle ikinci çalışmada ise

kompozit jel polimer elektrolitlerle ilgili testler yürütülmüştür. İlk adımda PAN ve PEG, dimetilformamid (DMF) polimer çözücüsünde çözünmüş ve 24 saat boyunca aralıksız karıştırılarak homojen çözeltiler elde edilmiştir. Bu basamakta PAN polimerinin çözeltideki kütlece yüzdesi sabit tutulup PEG yüzdesi değiştirilerek farklı kompozisyonlarda çözeltiler oluşturulmuştur. Daha sonra bu çözeltiler cam Petri kaplarına dökülmüş ve çözücü uçana kadar oda sıcaklığında bekletilmiştir. Elde edilen polimer filmler 15 mm çaplı diskler halinde kesildikten sonra 2 gün boyunca sıvı elektrolit içerisinde bekletilmiş ve jel formdaki elektrolitler hazır hale getirilmiştir.

Hazırlanan jel polimer elektrolitler, Fourier dönüşümlü kızılötesi spektroskopisi (FTIR) yöntemi ile yapısal ve termogravimetri/diferansiyel taramalı kalorimetri (TG/DSC) analizleri ile ısıl olarak karakterize edilmiştir. TG analizi kapsamında en yüksek bozunma sıcaklığı 339.8 °C ile en düşük oranda PEG içeren elektrolit için tespit edilmiştir. Bu elektrolitlerin oda sıcaklığındaki iyonik iletkenlikleri elektrokimyasal empedans spektroskopisi (EIS) yöntemi ile ölçülmüş olup en yüksek değer en fazla miktarda PEG içeren örnek için ve 5.56×10^{-3} S/cm olarak hesaplanmıştır. Elektrolitlerin Li^+ iyon transfer sayıları, EIS ve kronoamperometri tekniklerinin kullanılmasıyla elde edilen parametrelerle hesaplanmış olup artan PEG miktarı ile ters orantı göstermiştir. En iyi oksidasyon kararlılığı en yüksek iyonik iletkenliği de gösteren elektrolit örneği için 4.5 V u aşan düzeyde ve doğrusal taramalı voltametri (LSV) yöntemi kullanılarak ölçülmüştür.

İlk aşamadaki test sonuçları değerlendirilerek başlatılan ikinci aşamada, PEG oranının sabit tutulup dolgu malzemesi oranının değiştirildiği bir çalışma yürütülmüştür. Kompozit yapılı jel polimer elektrolitler için polimer çözeltisi hazırlama sırasında karışıma ek olarak SiO_2 dolgu malzemesi eklenmiştir. FTIR ve TG/DSC karakterizasyonları kompozit elektrolit örnekleri için de uygulanmıştır. En yüksek bozunma sıcaklığı 305.9 °C olarak ölçülmüştür. Bu elektrolitlerden yine EIS yöntemi kullanılarak 7.00×10^{-3} S/cm gibi oldukça iyi bir iyonik iletkenlik ölçümü yapılmıştır. En yüksek Li^+ iyon transfer sayısı ise PEG içermeyen elektrolit örneğinde olduğu gibi 0.89 olarak bulunmuştur. Elektrokimyasal kararlılık konusunda ise iki kompozit jel polimer elektrolit örneğinin 5 V u geçecek düzeyde oksidasyon kararlılığı gösterdiği tespit edilmiştir. Jel polimer elektrolitler için uygulanan testlerden farklı ve son çalışma olarak, uygun bulunan iki kompozit jel polimer elektrolit örneği, hazırlanan lityum kobalt oksit katot malzemesi ile birlikte yarı hücrede kullanılmış ve galvanostatik şarj-deşarj çevrim testine tabi tutulmuşlardır. Elektrolitlerin ilk çevrim profilleri oluşturulmuş ve karşılaştırılmıştır. Buna göre, bir hücrenin şarj kapasitesi diğerini neredeyse ikiye katlamış ve diğerinin şarj-deşarj eğrileri birbirine daha yakın çıkmıştır. Şarj kapasitesi ile ilgili olan ilk durum yüksek iyonik iletkenliğin bir sonucu olup iyonik iletkenliği 7.00×10^{-3} S/cm olarak ölçülen elektrolit örneği ile oluşturulan yarı hücre için elde edilmiştir. Şarj-deşarj eğrileri birbirine daha yakın olan yarı hücrenin durumu ise elektrokimyasal kararlılığı 5 V un üzerinde olan kompozit jel polimer elektrolite dayandırılmaktadır.

Sonuç olarak, çalışma kapsamında hazırlanarak karakterize edilen ve birtakım elektrokimyasal testlere tabi tutulan polimer bazlı jel ve kompozit jel elektrolitlerin lityum-iyon pil çalışmalarında kullanmak için potansiyel aday olabilecekleri değerlendirilmiştir. Konuyla ilgili sonraki çalışmalar, çoklu şarj-deşarj çevrim testleri ve deşarj kapasitesinin geliştirilmesi ile ilgili olmalıdır. Bu amaçla, farklı oranlarda dolgu malzemesi içeren daha fazla sayıda elektrolit örneği hazırlama, dolgu malzemesine yüzey modifikasyonları uygulama, farklı bir sıvı elektrolit kullanma,

aynı ya da farklı türde bir lityum tuzunu polimer çözeltisi hazırlama kısmında elektrolit içeriğine dahil etme vb. stratejilerle ileri çalışmalar yürütülebilir.

1. INTRODUCTION

As the energy demand rapidly grows to fulfil the needs of today's world, the corresponding storage of it has become prominent. The non-green, exhaustible and unsustainable identity of non-renewable resources has prompted the world to embark on a quest of alternative resources and to utilize them. By the *Net Zero Emissions Scenario*, global demand for electricity moves up to around 62,000 TWh in 2050 reaching almost 250% of its 2021 value. Additively, contribution of renewables to supply, rises from 28 to 88% with the same scenario pointing out the major direction change in energy resource choice [1]. In this regard, energy storage is the vital concern for renewable energy systems, considering the fluctuating character of certain types of resources, e.g. solar, wind etc.

Energy can be stored either chemically, electrochemically, electrically, mechanically or thermally. Falling into electrochemical energy storage systems, batteries convert chemical energy into electrical energy via electrochemical reactions [2]. They are being used in diverse applications such as power grids, electric vehicles, portable electronic devices, medical instruments, aviation, aerospace etc. [3]. Batteries are basically divided into two classes as primary (or non-rechargeable) and secondary (or rechargeable) that the former is for one time use while the latter is usable for multiple times [4].

Lithium-ion (li-ion) battery, as a rechargeable battery, has been leading the way in the area of portable electronics and electric vehicles (EVs). It is expected to be around 4,700 GWh of demand for li-ion battery by the year 2030 [5]. In Figure 1.1 below, it can be seen that the greater part of this demand is projected to belong to the transportation.

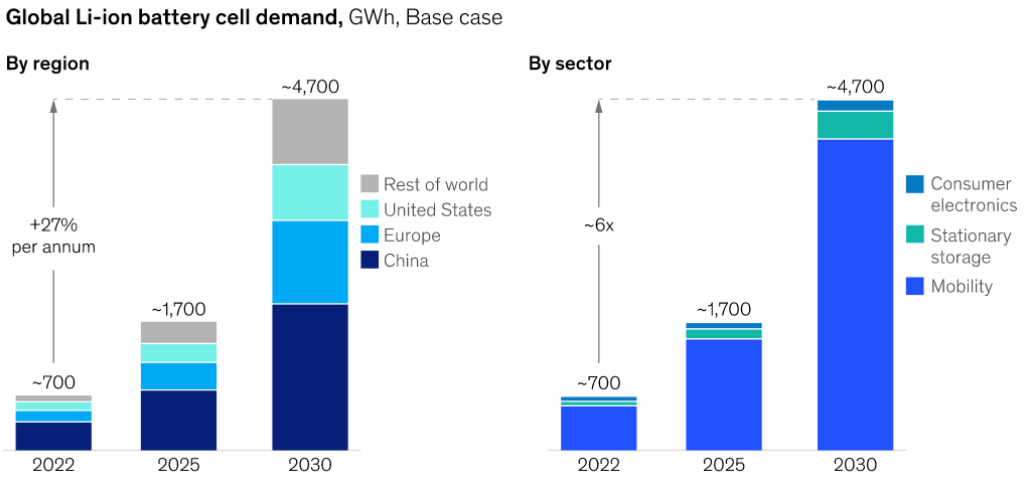

Figure 1.1 : Global demand for li-ion batteries over the next decade [5].

Some performance parameters are to be taken into consideration in li-ion battery operations, and these are basically energy density, cycle life, safety, charge/discharge rate, cost and ecological effect. Although each one of them has varying importance depending upon the application (e.g. energy density for portable electronic devices, cycle life for electric vehicles, etc.), the main goal is to improve them all as much as possible [6].

Conventional li-ion batteries have good cycle life, high energy density, and are functional at high level voltages as compared with previous designs. Notwithstanding, current li-ion batteries are converging their technological boundaries in terms of specific energy. Principally, EVs are foreseen to have over 500 Wh/kg energy density on cell basis in the future. Yet, current li-ion batteries have close to 300 Wh/kg. One of the solutions for high energy density is to employ high-capacity cathode materials in such a way that they require the anode side to hold a greater amount of lithium than usual which can be provided by applying the lithium-metal as the anode, as indicated in Figure 1.2. However, these alternative battery designs would suffer from major safety problems, e.g. short-circuit, thermal runaway and overheating. Additionally, there already exist some safety concerns of leakage, fire and even explosion which are directly related with the liquid electrolyte of the battery [7, 8]. Taking all into account, those collaboratively indicate that game changer developments are required in the battery field.

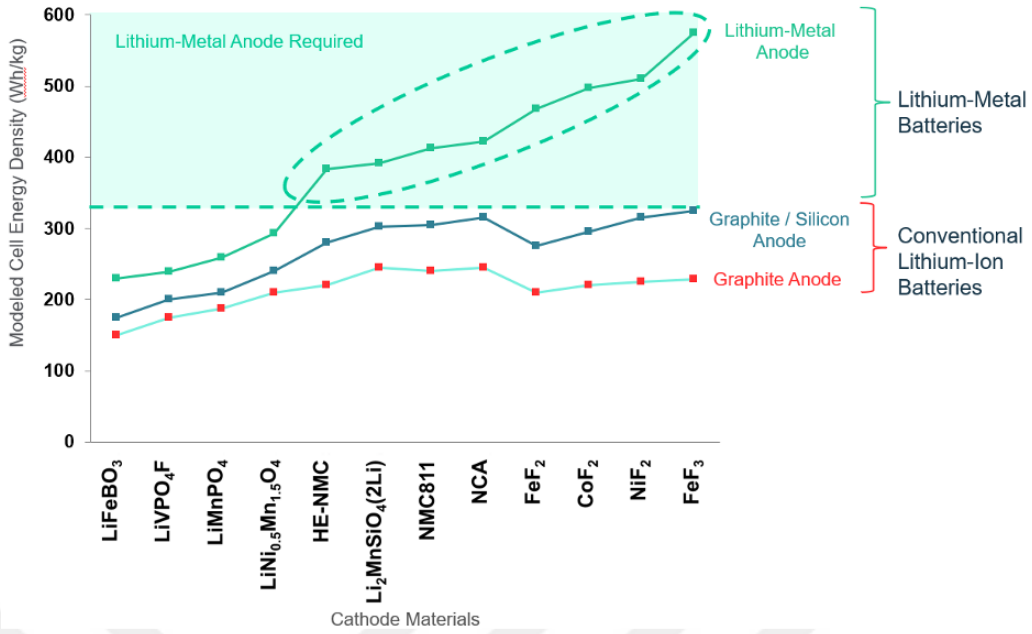

Figure 1.2 : A number of next generation cathode materials modelled with the conventional anodes and lithium-metal anode [9].

The aim of this study is to investigate the structural, thermal and electrochemical properties of the prepared gel polymer electrolytes with varying compositions for the li-ion battery applications.

2. LITERATURE REVIEW

2.1 Overview of Batteries

A battery consists of multiple cells which are formed by electrolyte and electrodes, namely anode and cathode, as shown in Figure 2.1. Conventionally, there exist a separator between electrodes, and current collectors in contact with each electrode to transmit electrons. Energy is stored through oxidation/reduction reactions taking place at the interfaces [10].

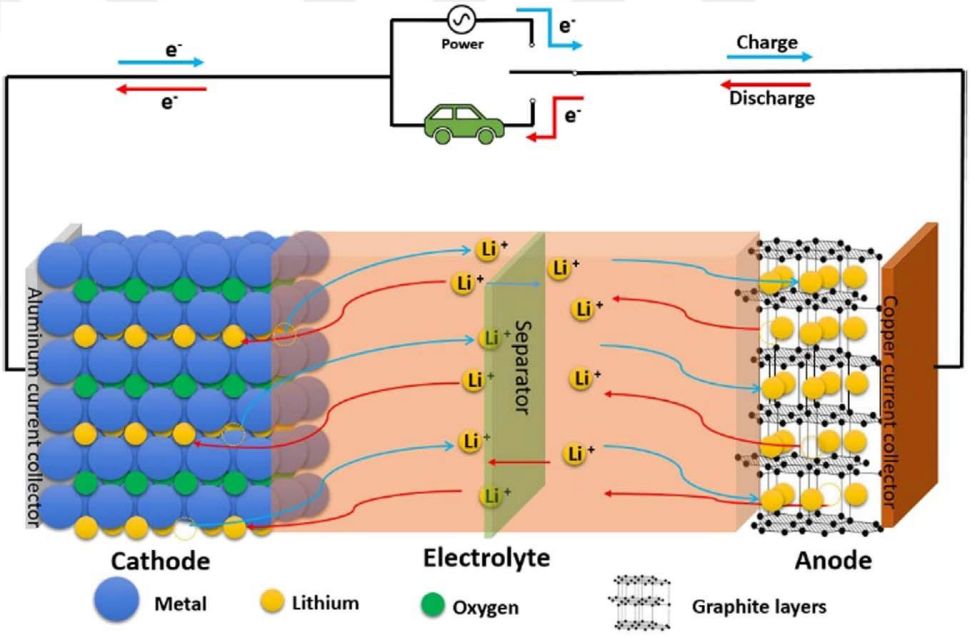

Figure 2.1 : Components and working mechanism of a lithium-ion cell [11].

In *discharging* process, the difference between chemical potentials of electrodes drives electrons to flow from anode to cathode via the external circuit while ions follow the same direction as the redox reactions take place. Inversely, ions and electrons separately flow towards anode from cathode in *charging* mode as a result of an applied voltage. Batteries are mainly divided into two groups: primary and secondary. The distinctive characteristic of secondary batteries is their rechargeability. Unlike one-time discharge property of primary batteries, rechargeable batteries are able to be reversibly charged and discharged [4].

Cycle stability, energy density, specific capacity, capacity retention and lifespan are among the performance parameters of the battery evaluation. Extensively used primary batteries are zinc-carbon (Zn-C), alkaline (Zn/MnO_2), zinc-air (Zn/O_2), silver-oxide (Zn/Ag_2O) and lithium (Li/FeS_2, Li/MnO_2, $LiSO_2$, etc.) batteries. Among the secondary batteries, lead-acid, nickel-based and lithium-based designs are distinguished [12-14].

2.1.1 Rechargeable batteries

In 1859, Gaston Planté invented the first lead-acid battery which was introduced into the market as the first commercial rechargeable battery. They still find place in current applications especially in portable electronic devices and automobiles, thanks to their features of high discharge current rate, low self-discharge rate, inexpensiveness and operability at relatively low temperatures. In a conventional lead-acid battery, lead (Pb) for anode, lead monoxide (PbO_2) for cathode and aqueous solution of concentrated sulfuric acid (H_2SO_4) for electrolyte are used. Lead-acid batteries have certain obstacles which restricts their use, and these involve high toxicity, low specific energy and low charging rate [15].

Later, in 1899, nickel-cadmium (Ni-Cd) battery was devised by Waldemar Jungner. It has longer cycle life, wider operating temperature window, faster charging, higher energy density by both gravimetrically and volumetrically. In a Ni-Cd battery, Cd, nickel oxide hydroxide NiO(OH), and alkaline potassium hydroxide (KOH) solution are used as anode, cathode and electrolyte, respectively. The modern sealed Ni-Cd battery began to be produced by 1950s, after beginning the applications of active material deposition on electrode and gas absorption during charging, making it favorite for portable devices until 1990s. However, they are required to be fully discharged before recharging which is related with the memory effect concept affecting their capacity. Other than that, toxic Cd and high rate of self-discharge made them unfavorable eventually. They are currently only being used in some portable devices [15].

Only by changing Cd with a hydrogen absorbing alloy, nickel-metal hydride (Ni-MH) battery was invented and commercialized in 1989. This less-toxic and less expensive design also yielded better performance in the manner of operating temperature window, cycle life, energy density, charging rate and memory effect comparing to Ni-

Cd battery. Ni-MH batteries had been utilized in hybrid electric vehicles and portable devices, yet they suffer from fast self-discharge, and gave place to li-ion batteries [15, 16].

Li-ion battery history started with practicing Li metal as anode. It is accounted as the ultimate anode owing to the lowest reduction potential (−3.04 V) and its high theoretical specific capacity (3860 mAh/g and 2061 mAh/cm^3). But it brings about destruction due to its high instability. As a milestone, the concept of shuttling of Li^+ ions based on reversible intercalation mechanism came to light in 1980s. In this concept, both of the electrodes are able to keep and release Li^+ ions without major structural change. Later, with the help of studies of Goodenough et al., Asahi Kasei Corporation made the first li-ion battery, based on graphite anode and lithium metal oxide cathode, and Sony Corporation commercialized it by using in the first mobile phone in 1991. This new design improved the battery in safety aspect, but energy density of the battery dramatically decreased because of the low theoretical capacity of graphite (372 mAh/g). In this respect, studies have been done mostly to promote the cathode side. Afterward, li-ion battery had begun to be gradually used in other electronic devices such as camera, PC, power tool, etc. and in EV/Hybrid-EV (HEV) [16-21].

Growing demand for portable electronics has drawn the attention on improving certain battery characteristics, particularly gravimetric energy density and cycle life. The breakthrough of li-ion battery facilitated the devices to be lighter than ever thanks to their high gravimetric energy density nearly doubling Ni-based batteries. Moreover, li-ion batteries have been increased threefold in voltage compared to the same group of batteries [15-17]. All those mentioned rechargeable battery types are comparatively given according to their certain characteristics in Table 2.1 below.

Table 2.1 : Certain characteristics of the main rechargeable batteries [15].

Characteristic	Lead-acid	Ni-Cd	Ni-MH	Li-ion
Gravimetric energy density (Wh/kg)	30-50	40-60	60-120	170-250
Volumetric energy density (Wh/L)	60-110	150-190	140-300	350-700
Battery voltage (V)	2.0	1.2	1.2	3.7
Cycle life (to 80% of the initial capacity)	300	1500	1000	500-2000
Fast charging time (h)	8-16	1	1-4	1 or less
Toxicity	High	High	Low	Low
In use since	Late 1800s	1950	1990	1991

2.1.2 Lithium-ion batteries

2.1.2.1 Cathode materials for li-ion batteries

Components of a li-ion battery should ensure various qualifications. These include low-cost, high-porosity, low-weight, suitability for lithium intercalation/deintercalation and compatibility of the electrode materials. Operation temperature, cell voltage, cycle life and capacity determine the choice of cathode. The inverse relation between capacity and cycle life is an important design issue to be succeeded in the way of effective li-ion batteries. From this aspect, layered lithium metal oxides ($LiMO_2$, M=Mn, Co and Ni), spinel lithium manganese oxide ($LiMn_2O_4$) and olivine lithium iron phosphate ($LiFePO_4$) are the three preferable structures for the cathode active materials. The crystal structures of these materials are given in Figure 2.2 [6, 18].

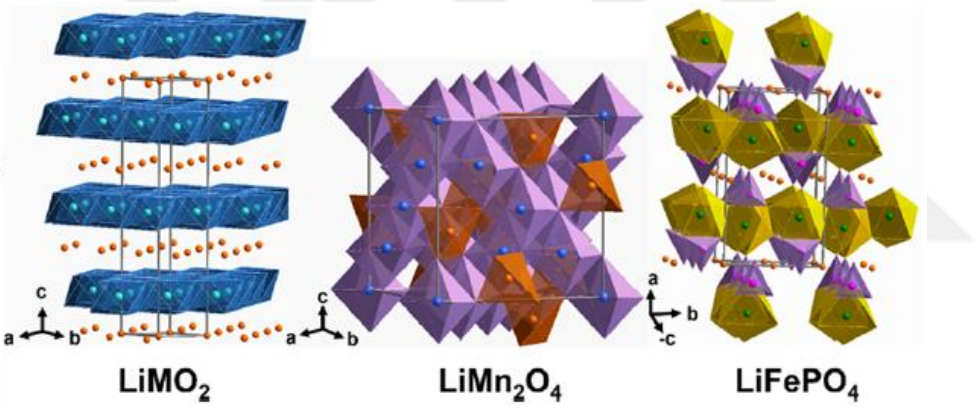

Figure 2.2 : Crystal structures of layered $LiMO_2$ (M= Mn, Co and Ni), spinel $LiMn_2O_4$ and olivine $LiFePO_4$ [6].

Having two-dimensional morphology, the highest practical capacity (~180 Ah/kg) belongs to $LiMO_2$ in the group. All three metals have different advantages and disadvantages (Co is the most toxic, Mn is the cheapest, etc.); hence the different complexes are practically used, e.g. lithium nickel manganese cobalt oxide ($LiNi_{1/3}Mn_{1/3}Co_{1/3}O_2$). These formations let the battery to have a higher gravimetric energy density and higher cycle number. These layered $LiMO_2$ batteries are rather being used in power tools. The crystal structure of spinel $LiMn_2O_4$ is in three dimensions and it has high stability against phase changes. Despite its high rate capability, this relatively cheap cathode active material falls behind the $LiMO_2$ regarding practical capacity (~120 Ah/kg). The olivine $LiFePO_4$ is eco-friendly, low-

cost and thermally highly stable by which it was allowed to be commercialized even though it is a material with comparatively low practical capacity (<160 Ah/kg) and low li-ion conductivity accompanying low discharge voltage. They are being used in EVs, HEVs, electric bikes and power tools. The highest crystal density among these crystal structures belongs to the layered $LiMO_2$ making it the one with the highest energy density [6, 16, 18].

2.1.2.2 Anode materials for li-ion batteries

Graphite, being more stable than Li metal, is compatible with widely used cathodes, and that allows it to be favored and be mostly used in the practical applications. Plus, it is superior in terms of discharge voltage and compensating current-voltage profile delivering high charge capacity. There are better alternatives to graphite in terms of capacity, yet gradual capacity loses and expansion problems are needed to be overcome [16, 18].

Because of the relatively poor capacity of graphite anode, some alloy anodes were developed. These easy to process alloys are outstanding in specific capacity, and mainly composed of Aluminum (Al), Magnesium (Mg), Tin (Sn) and Silver (Ag). During the charging/alloying process Li_nM (n>1 and M represents metal) is formed, and during the discharge it reverts back. Yet, huge volumetric change during lithium insertion/extraction, low electronic conductivity and corresponding capacity loss in the first cycle are said to be the drawbacks of this type of anodes. Having high theoretical specific capacities, conversion-type anode materials stand out with their fair cost and enhanced safety as they do not form lithium dendrites. Even though, the larger volume expansion and weak conductivity are the limiting factors for this type of anodes. Transition-metal sulfides, nitrides and oxides are listed among the conversion-type anode materials. As another kind, Silicon (Si) shows remarkable properties as an anode active material with its high capacity, low cost and abundancy. Still, there exist a couple of restricting matters like enormous change in volume throughout lithiation/de-lithiation and decrease in storage capacity in the first cycle. To overcome those problems, composite anodes consisting of Si and inert hosts were studied subsequently. Apart from aforementioned anode types, there are also novel carbon-based materials being studied as non-graphitic carbons with varying geometries such as carbon nanotubes, graphene and core-shell structures [22].

2.1.2.3 Electrolyte of li-ion batteries

The electrolyte of a li-ion cell is the medium where the ions transferred, and it basically consists of a separator and lithium salt dissolved in organic solvent(s), e.g. ethylene carbonate, propylene carbonate, dimethyl carbonate, diethyl carbonate, ethyl methyl carbonate. The salt (e.g. $LiPF_6$, $LiBF_4$, $LiAsF_6$, $LiClO_4$, $LiCF_3SO_3$) provides the ionic conduction within the cell while the polymer-based separator, such as polyethylene and polypropylene, located between the electrodes, prevents possible short circuits. There also could be organic compounds as additives in the electrolyte which have contribution to solid-electrolyte interface (SEI) formation, overcharging protection, etc., e.g. vinylene carbonate and biphenyl. This aforementioned liquid electrolyte is obliged to have a number of features so as to make a li-ion cell operate: high ionic conductivity, electrochemical stability to electrodes, being functional in a wide scale of temperature, being inexpensive and being quite safe in terms of fire, explosion, leakage, etc. [23].

Current collectors are electron conducting materials in contact with the cell electrodes. These materials are generally made of metals, and transmit electrons generated in electrode reactions from/to the external circuit. Conventionally, the slurry prepared for electrode material is coated on Aluminum (Al) for the cathode side and on Copper (Cu) for the anode side of li-ion batteries. A current collector should be very thin (10-20 μm), be electrochemically stable/compatible with the electrode's operating voltage, have high wettability and have good binding properties [23].

In spite of outperformance of contemporary li-ion batteries with liquid electrolytes over its predecessors, better cells need to be designed to overcome existing safety issues and to increase the energy density. Firstly, the liquid electrolytes have high toxicity and flammability. Further, energy density can be advanced by using high capacity materials for the electrodes which are not suitable with the common liquid electrolytes. They give rise to safety risks such as dendrite formation and anode expansion. When a high capacity anode material such as Li metal is used, high reactivity of lithium to the electrolyte creates needle-like growth called dendrites. These extensions cause reduction in capacity and eventually short-circuit. Lastly, if a cell is short-circuited, overcharged or exposed to high temperatures, uncontrollable reactions (e.g. decomposition of SEI, oxygen releasing exothermic reactions in cathode) start as the internal pressure devastatingly increase and suitable medium is

formed for fire and explosion, and this process is called as thermal runaway. To manage those drawbacks, some improvements may be applied at the level of individual components of the electrolyte including the use of more stable salts, stabilizers, additives, etc. Furthermore, next-generation designs, such as ionic liquids and solid or quasi-solid-state (gel) electrolytes are offered for the whole electrolyte component [7, 14, 24].

2.2 Solid-State Electrolytes for Li-Ion Batteries

Solid-state primary batteries find place in limited areas such as cardiac pacemakers, but the rechargeable solid-state batteries have not yet been used commercially. It is aimed for a rechargeable battery with solid-state electrolyte to have some qualifications, e.g. high energy density, low cost and high stability. Cells with solid-state electrolytes (SSEs) share the identical working principle with the cells having conventional liquid electrolytes. Thus, the solid-state electrolytes are expected to have some features of chemical stability to the environment, compatibility with the other parts of the cell, high Li^+ ion conductivity (over 10^{-4} S/cm at room temperature) and negligible electronic conductivity. Apart from this, they made it possible to construct a battery cell without using a separator by acting as one. The solid-state electrolytes proposed to be employed in li-ion batteries are mainly classified as ceramic-based, polymer-based and polymer/ceramic composites [25-28].

2.2.1 Ceramic-based (inorganic) solid-state electrolytes

Dating back to 1960s, the concept of solid-ion conductor suggested an alternative as it is not only safer and stable but also a threshold for higher energy densities in battery technology. The first solid electrolytes were based on conduction of Ag^+ and Na^+ ions followed by Mg^{2+}, O^{2-}, Li^+, etc. Ceramic-based SSEs are originated from the study on β-alumina ($Na_2O{\cdot}11Al_2O_3$) which is the first solid fast ion-conductor discovered. A ceramic ion conductor manages the transport according to the mechanisms for crystal structures which have lattice defects' tunnels that the ions move along. Elevated temperatures increase ion/vacancy concentrations; thus, the ionic conductivity increases as well [29, 30].

The type of the carrier, the type of the diffusion and the pathway for diffusion are the parameters regulating the Li^+ ion transport within a solid ceramic electrolyte. For

polycrystalline ceramic materials Li^+ ion transport realizes in three alternative modes as represented in Figure 2.3.

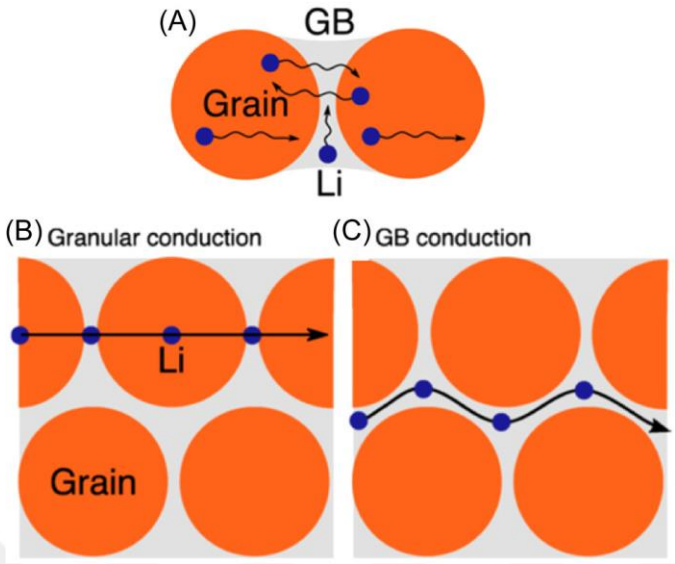

Figure 2.3 : Li^+ ion transport a) in grain boundaries, b) within grains and c) between grains [31].

Crystal structure defects such as point defects, volume defects, etc. determine the most of the ionic conduction in crystalline solids. Frenkel and Schottky defects of point defects are comprised of anion and cation vacancies or non-vacancies. Li^+ ion diffusion occurs as the ions shift to the neighboring vacancy from equilibrium position [32].

Fundamentally, the inorganic ceramic Li^+ ion conductors are grouped into two main categories: oxide-type and sulfide-type. The principal oxide-type conductors are NASICON, garnet and perovskite materials. Standing for sodium super ion conductor, termed according to $Na_{1+x}Zr_2Si_xP_{3-x}O_{12}$, and based on $AM_2(PO_4)_3$ formula, where A is for Li, Na or K and M is a cation of Ge, Zr or Ti , Li^+ ion conducting NASICON-type materials have three-dimensional (3D) crystal structure as shown in Figure 2.4a. $Li_{1+x}Al_xTi_{2-x}(PO_4)_3$ (LATP) and $Li_{1+x}Al_xGe_{2-x}(PO_4)_3$ (LAGP) are the two distinguished NASICON-type SSEs. They are made by partial substitution of Al for Ti or Ge in $LiTi_2(PO_4)_3$ and $LiGe_2(PO_4)_3$. Competing with liquid electrolytes, the highest ionic conductivity obtained from a NASICON material is in the scale of 10^{-3}-10^{-2} S/cm at room temperature by $Li_{1.3}Al_{0.3}Ti_{1.7}(PO_4)_3$. Nonetheless, they still have a couple of handicaps concerning interface stability and limiting their use in li-ion batteries with high energy-density [26, 31, 33].

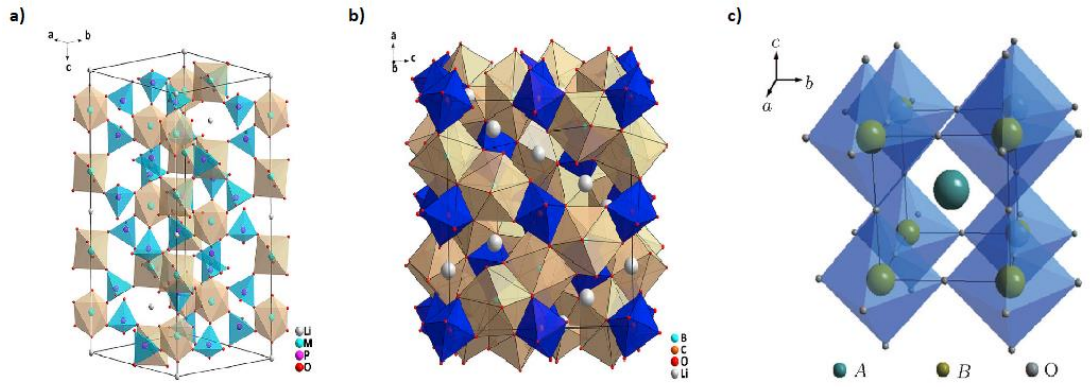

Figure 2.4 : The 3D crystal structures of oxide-type ceramic conductor examples: a) NASICON $LiM_2(PO_4)_3$ structure, b) garnet $Li_3B_3C_2O_{12}$ structure and c) perovskite ABO_3 structure [34].

Garnet-type SSEs have the general formula of $A_3B_2(XO_4)_3$ (A is Ca or Mg, B is Al, Fe, Ga, Ge, Mn or Ni, or X is Al, Ge or Si), and the first Li^+ ion conducting garnet-type material found is $Li_5La_3M_2O_{12}$ (M= Nb, Ta). Li^+ ion conducting garnets could be whether in tetragonal or cubic phase that differ in diffusion method. Ongoing studies are mainly focused on the garnet-type material of cubic $Li_7La_3Zr_2O_{12}$ (LLZO) which stands out with its relatively high ionic conductivity of 10^{-4}-10^{-3} S/cm at room temperature. Relatively good stability to Li metal and wide electrochemical window over 6V vs $Li|Li^+$ of garnet materials make them desirable to study on while they still suffer from interface problems [26, 31]. Figure 2.4b shows crystal structure of garnet-type materials in the form of $Li_3B_3C_2O_{12}$, where B is a four-coordination cation (e.g. La) and C is a six-coordination cation (e.g. Mb, Ta).

With the structure of ABO_3 (A is rare or alkaline earth metal and B is transition metal), perovskite-type inorganics initially were oxygen-ion conductors. Li^+ ion conductors are obtained later by partial substitution of A. For instance, a high Li^+ ion conductivity (over 10^{-3} S/cm) at room temperature is reached with $Li_{3x}La_{2/3-x}TiO_3$ (LLTO) formed by the occupation of A-sites by Li and La. Yet, LLTO failed towards lithium anode owing to high interfacial resistance and specifically the reduction of Ti^{4+} to Ti^{3+} by which electron conduction increases upon contact with the anode [26, 31, 33]. In Figure 2.4c, perovskite-type inorganic ceramic structure is demonstrated.

Being in the range of 10^{-4} to 10^{-3} S/cm at room temperature, the ionic conductivity of sulfide-type inorganic materials is attributed to weak bond between Li and Sulphur (S) which allows free moving of Li^+ ions and to the size of S ions which leads wide

migration tunnels for Li^+ ions. Sulfide electrolytes can be grouped as glassy, glass-ceramics and crystalline. The ionic conductivity for glassy sulfides is close to 10^{-4} S/cm while it is reaching almost 10^{-2} S/cm at room temperature for crystalline sulfides, e.g. lithium argyrodites (Li_6PS_5X, X=Cl, Br, I), thio-lithium superionic conductor (LISICON). On the other hand, glass-ceramics are relatively more compatible with Li metal anode yielding over 10^{-3} S/cm of ionic conductivity at room temperature. Even though the sulfides give fairly good room temperature ionic conductivity, and their chemical instability of H_2S generation could be overcome by adding certain nanoparticles to them, they still have trouble in electrode interfaces and consequent capacity loss [31].

2.2.2 Polymer-based (organic) solid-state electrolytes

The finding of ionic conductivity of polymers and subsequent application of them in electrochemical devices opened a new window into li-ion battery field with solid electrolytes. The ion transport in polymers is based on the free-volume model. Li^+ ions move between coordination sites of polymers' chains via free-volume (ion hopping) in amorphous regions, and thereby, the polymer chains experience segmental motion which could be facilitated by lower glass-transition temperature. For the crystalline phase of polymers, Arrhenius model involving activation energy rules the ion conduction contrary to segmental motion of amorphous zones. Nevertheless, ionic conduction in polymers mostly takes place in amorphous regions [23, 32, 33].

The preliminary study with polymeric ion conductors was based on a polymer-alkali metal salt complex in 1973, and it was applied to all-solid-state battery in 1979 as a polyethylene oxide-Li salt electrolyte [30]. Although polyethylene oxide is the most studied polymer as the solid electrolyte host by means of its high salt-solvating property, its low ionic conductivity (around 10^{-8} S/cm) at room temperature arising from its high crystallinity prompted other kinds of polymers to be worked on. Having functional polar groups, being highly salt-solvable and showing good compatibility with electrodes have determined the choice of polymers. In this context, poly(methyl methacrylate) (PMMA), polyacrylonitrile (PAN), polyvinyl alcohol, poly(vinylidene fluoride) (PVDF), poly(propylene carbonate) and poly(ethylene carbonate) could be numbered among these polymer hosts. [24, 26, 35]. Solid polymer electrolytes are superior to inorganic ceramics in terms of their flexibility and processability. But, they

possess relatively low Li^+ ion conductivity (less than 10^{-5} S/cm) at room temperature. [36]. For a solid polymer electrolyte, a number of conditions need to be met which are the ionic conductivity competing with conventional liquid electrolytes (greater than 10^{-4} S/cm at room temperature), the cation transference number, t_+, approaching unity (t=1) and high thermal/chemical/mechanical/electrochemical stability. [30]. To fulfill these necessities, there have been studies dealing with various electrolyte designs that could differ in polymer/salt kinds, synthesis methods, concentrations, etc. Considering those distinctions, polymer electrolytes for li-ion batteries can be fundamentally grouped as dry solid polymer, polymer-in-salt and single-ion-conducting polymer.

Dry solid polymer electrolyte is the basic system of a polymer matrix with a lithium salt dissolved in it. The complexes containing polyethylene oxide are the main examples for dry solid polymer electrolytes. In these systems, ion conduction takes place in the amorphous parts of the polymer where the temperature exceeds the glass-transition temperature of the polymer. As the glass-transition temperature of polymers is mostly far above the room temperature, and thus ionic conductivities at room temperature fall behind the desired values, practical use of this type of polymer electrolyte systems is not possible with their basic structures. Hence, several modifications such as blending, copolymerization, cross-linking have been applied to polymer hosts in addition to usage of advanced lithium salts and filler materials, all having the aim of reducing the crystallinity of the polymer to increase ionic conductivity at ambient temperature [35, 37].

Polymer-in-salt systems are considered as another group under polymer electrolytes. They are based upon the dry polymer electrolytes but they have higher concentrations of salt (more than 50 wt%) in their structures. The easier lithium salt and polymer matrix interaction increases the ratio of amorphous regions and enables ionic channels to occur, and results in elevated ionic conduction. PAN for instance, as one of the suitable polymers, has been used in such polymer-in-salt systems regarding its nitrile group in coordination with Li^+ ions. In spite of their relatively high ionic conductivity, they demonstrate poor mechanical stability to salt concentration increase. [35, 37, 38].

Single-ion-conducting polymer systems are designed for the purpose of blocking anion movement through electrolytes as it increases the cell impedance. This phenomenon is caused by the polarization that stems from anion migration to anode side while Li^+ ions are bound to polymer matrix. Accordingly, single-ion-conductors have been

designed to passivate anions by two particular mechanisms: attaching them to a polymer backbone and using receptors to immobilize them. [35, 37].

2.2.3 Polymer/ceramic composite solid-state electrolytes

Properties of solid polymer electrolytes could be enhanced by incorporation of other materials. One way is to realize this is integrating at least two types of polymers by blending, copolymerization or crosslinking. Simple mixing and dissolving of polymers in a common solvent is called as polymer blending. This method yields higher conductivity by reducing the crystallization. Copolymerization involves monomers of two or more different polymers which have abilities of facilitating ionic conduction or increasing mechanical stability. Crosslinking refers to promoting the ratio of amorphous phases to increase ionic conductivity, with linking polymer chains via covalent bonds [35].

Another way to improve solid polymer electrolytes is to convert them into composite form of different class of materials. The idea behind this approach is taking advantage of the upsides and hindering the downsides of both constituents via suitable procedures. Processability and cost-efficiency of polymer electrolytes could be collaborated with high ionic conductivity and rigidity of ceramic electrolytes. Built by combining polymer and ceramic components, composite polymer electrolytes are able to perform better interfacial stability toward electrodes, superior Li^+ ion transference number, adequate Li^+ ion conductivity at room temperature, etc. [39, 40]. To obtain composite solid electrolytes, inorganic fillers are reinforced into polymer structures. These active or inactive (inert) fillers are named on behalf of their role on ionic conduction in the electrolytes. Filler based arrangements can alter physical and chemical features of an electrolyte, and these are executed upon the concentration, geometry, morphology, etc. of the fillers. Active fillers themselves conduct Li^+ ions, and they yield high ionic conductivity and elevated Li^+ ion transference number. On the contrary, inert fillers do not directly engaged in ionic transportation. Instead, they behave as solid plasticizers [41].

Active fillers such as garnets, perovskites, sulfides, etc. contribute to the conduction, via their bulk structures as well as the interface developed between inorganic particles and polymers. Besides, particles are protected against possible chemical instabilities which is a major drawback for ceramic electrolytes, thanks to the polymer matrix. In

dimensional aspect, active fillers could be as particle, wire-like, sheet-like, or network-like. Although the composite polymer electrolytes containing active fillers result high ionic conduction and high Li^+ ion transference number, their complex synthesis restricts the studies [32, 42].

Even though ionic conductivities obtained by inert fillers are unfavorable comparing to those of composite polymer electrolytes containing active fillers, they stand out with their affordability and processability. They contribute lowering the glass-transition temperature of the polymer and plasticization of it. Moreover, based on Lewis acid-base theory, Li^+ ion conduction is increased by higher dissociation of Li salt via the functional groups of inorganic fillers. This also leads to a greater Li^+ ion transference number. Plus, they strengthen mechanical integrity of the electrolyte together with polymer matrix. Although most of the studies deal with nanoparticles, there are dimensionally various filler materials being studied to mostly compensate agglomeration caused by non-uniform distribution of them in polymer material. One-dimensional (1D) materials (nanotubes, nanofibers, nanorods, etc.) reduce the risk of agglomeration by supplying continuous interface. Additionally, to diminish the loss caused by unused inner part of particles and 1D fillers, two-dimensional materials, e.g. nanosheets, are proposed. But, they still need to be improved due to possible folding, curling and being located in such a way that blocking the Li^+ ion conduction [32, 39, 42].

Inert fillers used in composite polymer electrolytes are mainly metal oxides such as Al_2O_3, SiO_2, TiO_2, ZnO, etc., and some ferroelectric materials of $PbTiO_3$, $BaTiO_3$ and $LiNbO_3$. Other than these metal oxide fillers, clay materials like montmorillonite take place in recent studies as well. Metal oxide fillers reduce the crystallization, decrease the glass-transition temperature, and promotes the segmental motion of the polymer that have role on ion conduction. The first inert filler material used in composite solid electrolyte was Al_2O_3, and with SiO_2 they are the most studied ones owing to their role on chemical and electrochemical stability. As the interface developed by fillers has an effect on ionic conduction, the size, the amount and the shape, in terms of surface area, are also significant issues to consider for composite solid polymer electrolytes, e.g. using smaller particles result in higher surface area that supports the idea of using nano-sized particles. On the other hand, ferroelectric ceramic materials are as well used as inert fillers in composite solid electrolytes. They enhance ionic conductivity by

raising the dielectric constant, via polarization, of the polymer that they are in use [32, 39, 42, 43].

Apart from metal oxides, there are also molecular sieves, clays and even carbon-based materials as non-metal oxide fillers. Molecular sieves consist of uniformly distributed pores, and they could be classed according to the size of these pores, e.g. as micro-, meso-, macro-porous. These surface-area-increasing pores give rise to Lewis acidity to be high, and finally elevates the ionic conduction. As finely grained soil material, clays and more precisely layered nanoclays exhibit good performance on intercalation by changing cation and on dispersion through polymer. Montmorillonites are the typical example for layered nano clays, and they distinctively participate in ionic conduction via their nano-scale channels produced upon intercalation. Furthermore, normally used in anodes regarding its electrical conductivity, in some researches nanocarbon materials have been studied as electrolyte material. These carbonaceous components should be insulating such as graphene oxide, so that the electrical conduction is prevented. They promote the stability of the electrolyte both by thermal and interfacial aspects [32, 41].

Although composite solid electrolytes are constructed by using inorganic fillers by dispersing them through a polymer matrix, there are also novel studies applying alternative approaches such as layered structures, 3D networks and open-framework. Layered structures are configured heterogeneously as consisting of separated layers of polymer electrolytes and ceramic electrolytes. In addition to the general advantages of using both, interfacial issues like poor contact, side reactions, lithium dendrite growth, etc. could be minimized by these double-layered or three-layered (sandwich) structures. As another design, 3D networks are formed in such a manner that the opposite logic of regular composite solid polymer electrolytes. In this arrangement, frameworks are based on inorganic materials creating non-intersecting conduction channels while the polymer occupies the void. This distinguished design yields higher ionic conductivity than the other geometries. Open-framework-related composite electrolytes are metal-organic frameworks, covalent organic frameworks and porous organic cages. Metal-organic frameworks have very high porosities and internal surface areas. The electrolytes with covalent organic frameworks could be either in all-solid-state or in solid-like-state. Differently, porous organic cages are based on

polymer crystalline network and ionic conduction is supplied via this network in collaboration with hydrated salt over it [32].

Solid composite polymer electrolytes are synthesized mainly by four techniques: solution casting, mechanochemical method, infusion and 3D printing. Solution casting is the most favorable and applicable method based on solvent evaporation from solid electrolyte mixture of preferred form, e.g. thin film. In mechanochemical method, there is no use of any solvents, and thus it is a favorable process for compounds that are sensitive to organic solvents, e.g. sulfide-type inorganic electrolytes. If a polymer solution is infused into inorganic solid electrolyte framework, and then the solvent is evaporated followingly, it is called as infusion method. This technique facilitates continuous Li^+ ion conduction. Not yet being put into full practice, 3D printing aims to integrate the electrolyte with the electrodes in peculiar shapes. In the studies concerning this method so far, reduced interfacial resistances were obtained [26].

2.3 Gel Polymer Electrolytes

Even though all-solid-state electrolytes are the desired form for future li-ion batteries, their current ionic conductivities at room temperature fall behind the practical limits for mass production. In order to increase the ionic conductivity, plasticizing agent addition has been a major practice which creates gel polymer electrolytes. This so-called intermediate or quasi-solid state between liquid and all-solid electrolytes, first proposed by Feuillade et al. in 1975, is mainly comprised of polymer, lithium salt and plasticizer. Unlike the way in solid polymer electrolytes, conduction of ions in gel polymer electrolytes is governed mostly by liquid phase and to a lesser extent by swollen phase of polymer matrix through liquid electrolytes. Depending on the form of gel electrolyte, it could be the liquid phase ruling the ion conduction if microporous structure exists or the swollen gelled phase where the ions are transferred. They exhibit the key features of cohesiveness (yielding improved stability) and diffusivity (yielding high ionic conductivity) of solid and liquid electrolytes, respectively [24, 31, 37]. A comparison between liquid, solid polymer and gel polymer electrolytes in terms of their advantages and disadvantages is given in Table 2.2 below.

Table 2.2 : The advantages and disadvantages of liquid, solid polymer and gel polymer electrolytes [43, 44].

Electrolyte Type	Advantages	Disadvantages
Liquid	high energy density, good electrode contact outstanding rate capability	unavoidable dendrite formation, insufficient electrochemical stability, poor safety
Solid polymer	high safety	inadequate cycle performance, low ionic conductivity, weak electrode compatibility
Gel polymer	less dendrite formation, higher safety, flexibility, processability	poor mechanical strength

Polyethylene oxide, poly(vinylidenefluoride), PMMA, PAN and poly(vinylidene fluoride-hexafluoropropylene) are among the polymer matrices employed in gel polymer electrolytes with moderate to high ionic conductivity values at ambient temperature (~10^{-4}-10^{-3} S/cm) approaching to that of the liquid counterparts [30]. The aforementioned ion conduction mechanisms are based on physical states of gel polymer electrolytes: homogeneous or heterogeneous. Homogeneous gel polymer electrolytes are uniform, and the ion transport is dominated by whole gel phase. On the contrary, multiphase heterogeneous gel electrolytes manage ion conduction mainly with liquid electrolytes. They need to be porous enough to uptake a considerable amount of liquid electrolyte, but the pores are required to be micro level in order to prevent possible leakage. Casting and in-situ polymerization are the common procedures for preparing homogeneous gel electrolytes while heterogeneous gel electrolytes are usually prepared via phase inversion, electrospinning and foaming methods [37].

The improvement in ionic conductivity by the addition of plasticizer stems from the correlated increase in amorphous phase, the boost in segmental motion and the easier dissociation of salt. Organic solvents, low-molar-mass organics and ionic liquids are the three kinds of plasticizers. Organic solvents should have high dielectric permittivity and low viscosity so that they could make salt solution and Li^+ ion transportation easier. Ethylene carbonate (EC), diethyl carbonate (DEC), dimethyl

carbonate (DMC), propylene carbonate (PC) and γ-butyrolactone are the leading organic solvents that are used as plasticizer in li-ion batteries. Polyethylene glycol (PEG), polyethylene glycol dimethyl ether, borate esters and phthalates are considered as suitable organic plasticizing compounds having low-molar-masses. Chemical, thermal and electrochemical stabilities of ionic liquids have made them a fascinating alternative for use as plasticizers. These room temperature molten salts have units of organic cation-inorganic anion couple. [31, 37].

Adding the plasticizer to the polymer backbone reduces the mechanical stability of a solid electrolyte that may cause safety issues. The properties of plasticized solid electrolytes could be enhanced by the beforementioned polymer modifications of blending, copolymerization and crosslinking. Moreover, the incorporation of inorganic materials could be also an improvement regarding the mechanical stability of gel polymer electrolytes as such in composite solid polymer electrolytes. Therefore, the composite electrolyte making and the overall effects of the process are similar for solid and gel polymer electrolytes. One special subject to mention is that the inert fillers used in composite electrolyte structures individually behave as plasticizers. Hence, gel polymer electrolytes may be grouped as plasticizer-including, inorganic filler-including and a combination of plasticizer/inorganic filler including gel polymer electrolytes. The ion conduction based on free-volume model in polymers greatly takes part in composite gel polymer electrolytes since the ceramic components facilitate the diffusion of Li^+ ions by maximizing the free volume. The improved safety and performance of composite gel polymer electrolytes stem from the fact that the filler materials help to prevent the lithium dendrite growth via confining the liquid electrolyte within the gel complex structure [41, 44].

Particle morphology, particle size and concentration are essential criteria to consider when designing composite gel polymer electrolytes with inorganic fillers. Particle concentration increase have a positive influence on ionic conduction to some extent. Directly proportional relation between the concentration and ionic conduction transforms into reciprocal proportion after some point because of agglomeration. Therefore, particle concentration is an important parameter to sustain mechanical stability of the composite electrolyte. On the other side, considering agglomeration in another aspect, particle size is need to be mentioned. Although inert nanoparticles result higher surface area, they are prone to agglomerate which limits their amount

within the structure. However, the usage of plasticizers, which decreases the crystallization and increase salt dissociation, compensate this adverse impact [42]. Consequently, it can be concluded that there is a mutual supportive relation between inert fillers and plasticizers as the former strengthen the mechanical structure weakened by the plasticizer and the latter eases the dispersion of the inert filler.

3. EXPERIMENTAL STUDY

3.1 Materials

The electrolyte samples were prepared from polyacrylonitrile (PAN, M_w=150,000 g/mol) as polymer host, polyethylene glycol (PEG, M_w=1,500 g/mol) as plasticizer, N,N-Dimethylformamide (DMF) as polymer solvent, silicon dioxide (SiO_2, 10-20 nm) as inorganic filler material and lithium hexafluorophosphate solution in organic solvent mixture of ethylene carbonate, diethyl carbonate and dimethyl carbonate (1M $LiPF_6$ in EC/DEC/DMC=1:1:1 (v/v/v)) as liquid electrolyte. No treatment was applied to the chemicals.

Additionally, half-cells with the composite gel polymer electrolytes were assembled by using lithium cobalt oxide ($LiCoO_2$) cathode and lithium anode. The cathode was prepared by using $LiCoO_2$ powder (LCO) as active material, carbon black (CB) as conductor, poly(vinylidene fluoride) (PVDF) as binder, with LCO/CB/PVDF=70:20:10 in weight and N-Methyl-2-Pyrrolidone (NMP) as solvent. CR2032 components, i.e. cases, spacers and springs, were used for the coin cell structure.

3.1.1 Polyacrylonitrile

PAN is a suitable polymer host material as it supplies outstanding compatibility with the lithium-containing-electrodes, wide electrochemical stability window, adequate thermal stability and high ionic conductivity in the battery it is applied. This flame-resistant and easily processable semicrystalline polymer material also facilitates the ion solvation. The PAN polymer chains, displayed in Figure 3.1, involve electron withdrawing nitrile group (C≡N) that increase the electrochemical stability of the battery structure [45, 46].

3.1.2 Polyethylene glycol

The low-molecular-weight PEG, given in Figure 3.2, is considered as a compatible material among the plasticizers to be used in battery since it provides safer working

conditions by means of its non-volatility. It promotes ionic conduction via making the electrolyte more amorphous [48, 49].

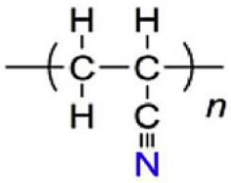

Figure 3.1 : The chemical structure of PAN polymer matrix [47].

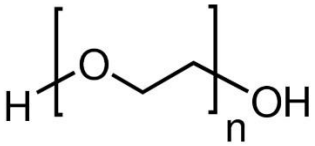

Figure 3.2 : The unit structure of a PEG molecule [50].

3.1.3 Dimethylformamide

In spite of strong dipole-dipole interactions between PAN molecules caused by its nitrile groups, DMF is a favorable solvent owing to the lone pairs of nitrogen atoms. This volatile solvent is also suitable for SiO_2 dissolution [51, 52].

3.1.4 Silicon dioxide

The electrochemical properties of solid polymer and gel polymer electrolytes can be enhanced by the addition of SiO_2 powder. It implicitly contributes ionic conductivity of the electrolyte it is in by the Lewis acid-base interactions formed between the silica's polar surface groups, represented in Figure 3.3, and ions, and by decreasing the polymer crystallinity. Moreover, better interface contact between electrode and electrolyte is provided. Besides, the SiO_2 particles act as insulators by blocking the possible side reactions between electrodes and impurities within the electrolyte, if any [42, 52, 53]. The employment of the SiO_2 in a nano-sized level is for taking advantage of the enlarged surface area.

Figure 3.3 : The chemical structure of silicon dioxide [54].

3.1.5 $LiPF_6$ in EC/DEC/DMC

1M $LiPF_6$ in EC/DEC/DMC=1:1:1 (v/v/v) solution as the liquid electrolyte was entrapped in the prepared polymer and composite polymer samples by immersing them in it.

Although $LiPF_6$ salt limits the advantages of using the solution due to its sensitivity to moisture and decomposing to toxic HF, this liquid electrolyte is a very common type that is being used in lithium-ion batteries. The excellent ionic conductivity, good stability to high-voltage cathodes and favorable interface layer between graphite anode (solid-electrolyte interface), which is important for charge/discharge cycle performance, are the main causes behind the interest [55-57].

3.2 Preparation of Gel Polymer Electrolytes

The gel polymer electrolyte samples were fabricated via solution casting and following dipping into the liquid electrolyte. First, the dry films were obtained by dissolving PAN and PEG in DMF and stirring continuously for about 24 hours to obtain homogeneous solutions. In this step, SiO_2 powder as filler material was optionally added to the polymer solution, and mixed together to get the composite polymer solutions. Then, the solutions were cast in glass Petri dishes of 45 mm in diameter, and left for the solvent evaporation at room temperature. After that, the obtained films were cut into discs of 15 mm in diameter, and immersed in the liquid electrolyte for about 2 days. This stage was realized in an Argon filled glove box [45, 58, 59]. The casting solution compositions of the gel and composite gel electrolytes are listed in Table 3.1 and 3.2 below, respectively.

Table 3.1 : Compositions of the casting solutions for the gel polymer electrolytes.

Sample	PAN (wt%)	PEG (wt%)	DMF (wt%)
PAN	10	0	90
S1	10	3	87
S2	10	5	85
S3	10	7	83
S4	10	10	80

Table 3.2 : Compositions of the casting solutions for the composite gel polymer electrolytes.

Sample	PAN (wt%)	PEG (wt%)	SiO_2 (wt%)	DMF (wt%)
C1	10	5	0.5	84.5
C2	10	5	1	84
C3	10	10	0.5	79.5
C4	10	10	1	79

3.3 Characterization of the Electrolyte Samples

3.3.1 Fourier transform infrared spectroscopy

Fourier transform infrared spectroscopy (FTIR) as a non-destructive technique is based on irradiation of a sample, and is used to characterize materials by the identification of molecular structures via measuring the infrared spectrum. The spectrum gives light intensity measurement values with respect to the given light property [60]. In this study, it is the plot of wavenumber (cm^{-1}) versus transmittance (%). Specific molecular bonds are determined by the signal peaks that indicate vibrations of these bonds at specific wavenumbers, and these peaks are the fingerprints for the bonds. Apart from the molecular identification, the interactions between different functional groups can be detected. Therefore, the possible changes and complexations either by ion dissociation or by the addition of plasticizer and filler to the polymer host can be observed. These are observed as the new band formation, band shifting and band intensity change [61, 62].

For the sample analysis, mid-IR spectrum (4000-400 cm^{-1}), demonstrated in Figure 3.4, is generally used, and it is investigated in four sub-regions: single-bond (4000-2500 cm^{-1}), triple-bond (2500-2000 cm^{-1}), double-bond (2000-1500 cm^{-1}) and fingerprint (1500-600 cm^{-1}) [63].

The transmission FTIR spectra analyses of the gel and composite gel polymer electrolytes were performed by using a Perkin Elmer Spectrum One Spectrometer and the recordings were done in the range of 4000-650 cm^{-1}.

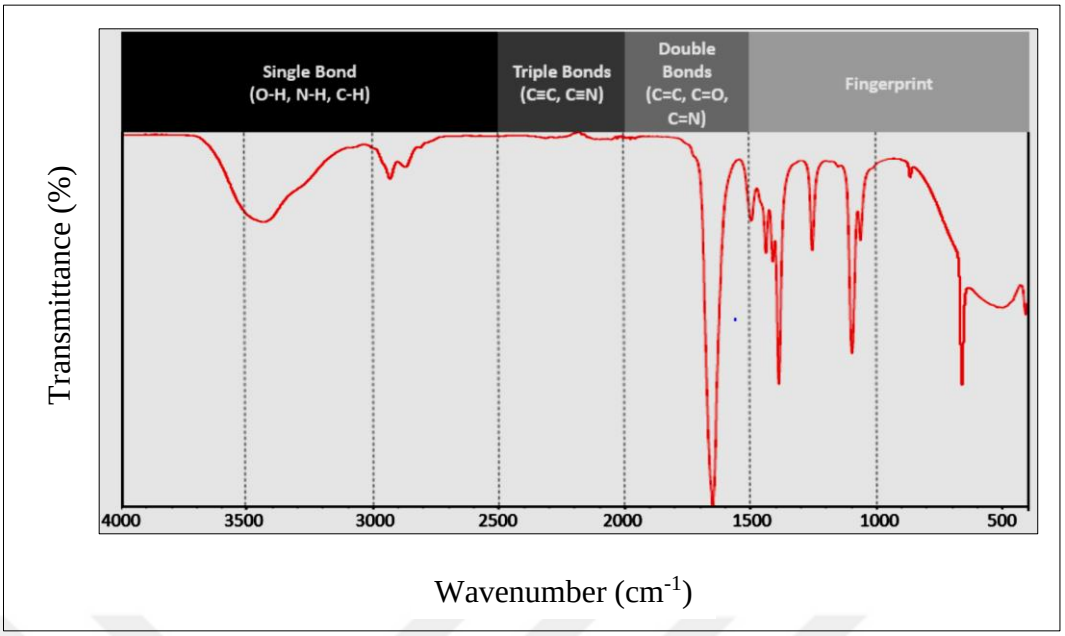

Figure 3.4 : A typical mid-IR transmission spectrum [63].

3.3.2 Thermogravimetry and differential scanning calorimetry

Thermal analysis techniques of thermogravimetry (TG) and differential scanning calorimetry (DSC) are used to investigate thermal behavior of the materials. TG is performed to characterize materials with regard to thermal stability through stages of weight gain or loss under gradual temperature change. Generally, the mass loss is observed through heating under an inert atmosphere. The content of volatile compounds present in a sample and the decomposition temperature can be determined. Thermal properties of polymeric materials based on degradation mechanism, chemical compositions and weight loss in a given temperature range are studied in TG. DSC gives information on thermal changes as heat flow through the interval of temperature and/or time. Glass transition temperature (T_g), melting temperature, specific heat capacity, etc. and phase-change behavior of polymeric materials can be identified via DSC [64].

In the present study, TG and DSC were carried out to examine the effects of plasticizer and filler at varying concentrations on the thermal properties of the prepared samples. TG and DSC techniques for thermal analyses of the electrolyte samples were conducted using a TA Instruments SDT-Q600 Simultaneous TG/DSC Analyzer under nitrogen gas flow with 10 °C/min of scan rate.

3.3.3 Electrochemical measurements

The measurements for ionic conductivity, transference number and electrochemical stability were performed by using Gamry Interface 1010E Potentiostat/Galvanostat/ZRA Instrument, and half-cell cycle tests were applied by using MTI BST8-WA battery analyzer in connection with a computer for data acquisition.

3.3.3.1 Ionic conductivity

The ionic conductivity, σ, of a solid or solid-like electrolyte material can be found based on the formula given in equation (3.1) below.

$$\sigma = \frac{l}{R_b \times A} \tag{3.1}$$

where l is the thickness of the electrolyte material, A is the surface area of the electrolyte material in contact with electrode and R_b is the bulk resistance of the electrolyte which is determined via electrochemical impedance spectroscopy (EIS) [65]. EIS is measured to obtain the impedance (Z) of the dielectric materials, and it is plotted as the function of frequency. The cell with the sample is subjected to small AC signal to avoid polarization, and each impedance respond with real (Z') and imaginary (Z") parts belongs to a specific frequency point. All the points corresponding a given range of frequency results the Z' vs Z" complex impedance plot, i.e. Nyquist plot [66]. Nyquist plot for ideal systems would be a perfect semicircle, a vertical line or a combination of them as shown in Figure 3.5. But for the real systems, the plot is mostly a depressed semicircle and an inclined straight line. The x-intercept of their intersection point gives the R_b value. Moreover, the semicircle can completely disappear for the conditions enabling facile ion transportation, and R_b is directly taken as the x-intercept of the low frequency line [65, 67, 68]. The semicircle demonstrates the conduction process in the electrolyte while the spike belongs to charge accumulation at the interface between electrolyte and electrode. The resistance values are found by fitting the obtained plot in accordance with equivalent electrical circuits. The Z' and Z" correspond to resistive and capacitive elements, respectively. Therefore, a semicircle is represented by a resistor and a capacitor in parallel while a spike by only a capacitor. The capacitor is changed with a constant phase element in real

systems because of surface roughness of the materials and nonuniform distribution of the charges [69, 70].

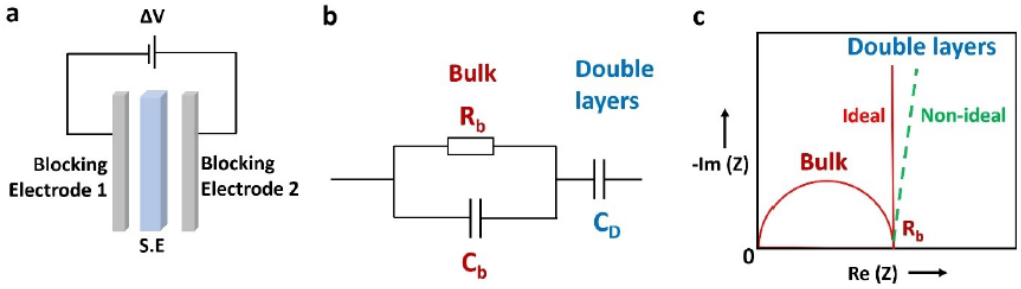

Figure 3.5 : Ionic conductivity measurement. a) Cell configuration with solid electrolyte and blocking electrodes. b) Equivalent circuit representation. c) Nyquist plot of the equivalent circuit for ideal systems and the change for real systems [65].

The results for ionic conductivity were obtained as Nyquist diagram based on EIS which plots the impedance response of the cell as the function of frequency. The tests were performed between 0.1 Hz-1 MHz under 5 mV of AC voltage by placing each of the films between two ion-blocking stainless steel electrodes.

3.3.3.2 Cation transference number

For a polymer-based electrolyte, the ionic conduction is expected to be supplied mostly by cations. Therefore, cation transference number (t_+) is an important indicator for lithium-ion batteries especially in terms of cycle stability. This number demonstrates the quality of salt dissociation as the anions are needed to be immobilized with polymer host in order to prevent the polarization, and so the cations provide the conduction. The polarization is caused by decomposition of the anions, which are transferred through electrolyte, on the positive electrode. Contrary to cations, anions do not involve in redox reactions and cause concentration gradient at the interface resulting the polarization. This phenomenon gives rise to higher internal resistance and lower discharge capacity for the cell. For an ideal electrolyte with completely stationary anions, the cation transference number would be equal to one. Hence, an electrolyte with a high t_+ value propose reduced electrode polarization and improved cycle stability [14, 59, 71].

Based on single salt system, the Li^+ transference number (t_{Li+}) can be estimated by using a combined measurement technique proposed by Evans et al. Assembled by locating the electrolyte film between two non-blocking electrodes of lithium metal, the

cell is subjected to DC polarization under constant low voltage. This method is called chronoamperometry. The ratio of the steady-state current reached at the end to the initial current basically gives the transference number. However, the voltage drop should be considered as the interfacial resistance increases through the process. Hence, the coefficients with initial and final interface resistances are measured by AC impedance spectroscopy, and used in the calculation of t_{Li+}. The equation for t_{Li+} is given as in the following equation (3.2).

$$t_{Li^+} = \frac{I_{ss}(\Delta V - I_0 \cdot R_{i,0})}{I_0(\Delta V - I_{ss} \cdot R_{i,ss})} \quad (3.2)$$

In the equation, I_{ss} is the steady-state current, I_0 is the initial current, $R_{i,0}$ is the initial interfacial resistance, $R_{i,ss}$ is the steady-state interfacial resistance and ΔV is the step voltage [59, 71]. In the study, step voltage is 10 mV of DC voltage for chronoamperometry while the frequency range and the AC voltage for EIS measurements are 0.1 Hz-1 MHz and 5 mV, respectively.

The t_{Li+} of most liquid electrolytes is less than 0.5, and a gel polymer electrolyte should have a higher value in order to avoid unstable and inhomogeneous ion deposition [72, 73].

3.3.3.3 Electrochemical stability window

For the possible practical application of a battery it is important to have knowledge about its electrochemical stability. Electrochemical stability window (ESW) of the cells with the samples was inferred from linear sweep voltammetry (LSV) method by placing each sample between an SS as the working electrode and a lithium metal foil as the counter electrode. In this technique, the cell is subjected to an increasing voltage with a constant rate to detect the onset current value which corresponds to bulk oxidation, i.e. decomposition, of the electrolyte. It gives the maximum working voltage for the cell, and further this point the cell is no longer operable and stable. Considering the aim of usage of high-voltage cathodes, the electrolytes are needed to have wide ESW which requires the maximum possible onset current value [35, 45, 61, 71].

One crucial matter to concern about is keeping the voltage sweeping low so as not to deviate from equilibrium through the measurement. The maximum voltage is inferred

from the sudden increase in the current [61]. In the study, the LSV tests were conducted between 2.5-6 V with 5 mV/s of scan rate at room temperature.

3.3.3.4 Half-cell performance

The galvanostatic charge-discharge cycling is a method to evaluate the capacity and cycle stability of a battery when a new material is used as a battery part, i.e. electrode, electrolyte etc. It was applied to the half-cell with the most favorable composite gel polymer electrolytes according to the other characterization results. This battery cell was arranged in such a way that $LiCoO_2$ and lithium foil were used as the working and reference electrodes, respectively. The half-cells were cycled at room temperature, within 2.5-4.2 V (vs. Li^+/Li) and at 0.1C rate which means consecutive 10h charge and 10h discharge for one cycle was hypothesized. The theoretical capacity C is calculated by the multiplication of the specific theoretical capacity and mass of the active material [74].

4. RESULTS AND DISCUSSION

4.1 Results for the Gel Polymer Electrolytes

4.1.1 FTIR analysis of the gel polymer electrolytes

FTIR studies were carried out to investigate the chemical interactions and structural changes of the constituents of the prepared electrolyte samples to have knowledge about their compatibility. The fundamental vibrational modes seen at the specific wavenumbers, found on literature, of the main constituents of the gel polymer electrolytes are listed in Table 4.1 below.

Table 4.1 : Wavenumbers correspond to vibrational modes for PAN and PEG based on literature data.

Material	Wavenumber (cm^{-1})	Band Assignment
PAN	1074	C-C stretching [68]
	1227	C-H bending in CH [75]
	1454	C-H bending in CH_2 [75]
	1733	C=O stretching [75]
	2243	C≡N stretching [75]
	2812	C-H stretching in CH [68]
	2940	C-H stretching in CH_2 [75]
	3480	N-H stretching [75]
PEG	1094	C-O-C stretching [76]
	1240	C-O stretching [77]
	1279	O-H stretching [78]
	1343, 1464	C-H bending [78]
	2878	C-H stretching [78]
	3441	O-H stretching [78]

The structural effect of PEG addition to PAN was examined, and FTIR spectra is given as in Figures 4.1 and 4.2 for dry polymer film samples and their corresponding wet versions, obtained by immersing into the liquid electrolyte, respectively. For pure PAN

sample C-C stretching vibration peak is at 1073 cm^{-1}. It shifts to 1074 cm^{-1} for the sample S1, and disappears for the other samples. Similar situation rules for the peaks of C-H bending in CH by a change from 1233 cm^{-1} to 1234 cm^{-1}. The vibrational peak for C-H bending in CH_2 is seen to unchanged for the sample S2 at 1454 cm^{-1}. Though, it shifts up to 1455 cm^{-1} for the samples with other compositions. Additionally, the peak intensities for the samples S3 and S4 are decreased for C-H bending vibration in CH_2. The vibrational peak of C=O stretching gets shifted from 1737 cm^{-1} to 1738 cm^{-1} for the sample S4. The change from 2242 cm^{-1} to 2243 cm^{-1} in the characteristic C≡N stretching vibration of PAN is seen for all the samples except S1. The C-H stretching vibrations in CH and CH_2 at 2812 cm^{-1} and 2935 cm^{-1} for pure PAN are both observed to vanish for the samples S2 and S4. Lastly, the peak at 3482 cm^{-1} for pure PAN assigned to N-H stretching vibration changes and appears at lower wavenumbers for all the samples.

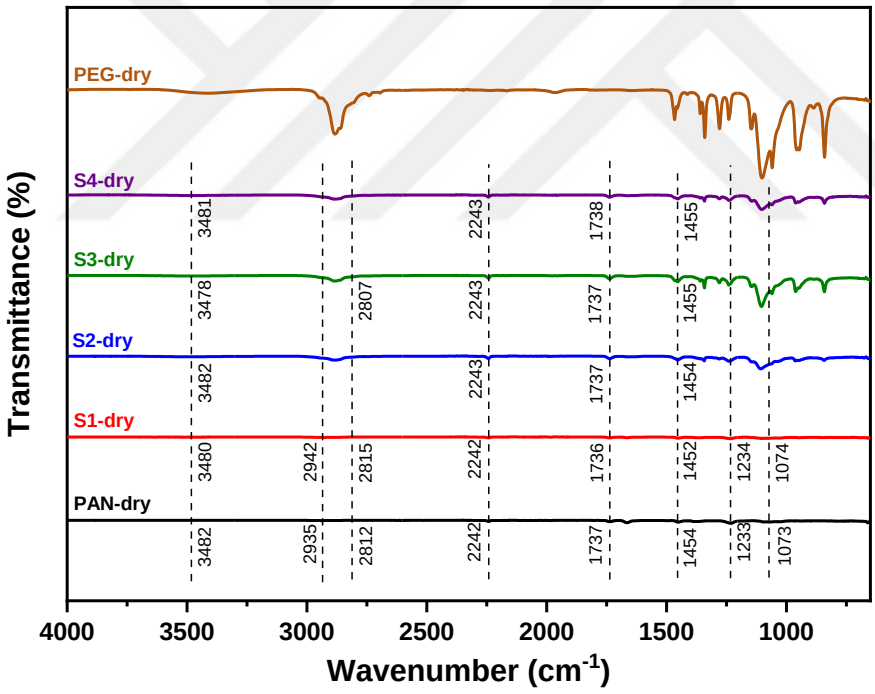

Figure 4.1 : FTIR spectra of the dry polymer samples PAN, PEG, S1, S2, S3 and S4.

The other peaks not mentioned belong to PEG, and these are C-O-C symmetrical stretching at 1102 cm^{-1}, C-O stretching at 1240 cm^{-1}, O-H stretching at 1279 cm^{-1}, C-H bending at 1341 and 1467 cm^{-1}, C-H stretching at 2883 cm^{-1}, respectively, for pure PEG. Those peaks are clearly seen also for the samples S2, S3 and S4. The reduce in intensity and vanishing of the peaks indicate the consistency of PAN and PEG. No

new peaks are developed for the samples with both PAN and PEG and this points out that there is only physical interaction between the two polymers [79]. On the other hand, the characteristic bands of the PAN and PEG are mainly preserved upon mixing that facilitate the prospective interactions between the polymer structure, liquid electrolyte and nanofiller [80].

In Figure 4.2, the combined FTIR graphs of the wet samples with varying compositions are given and investigated. Assigned to the C=O stretching vibration which is arising from organic compounds in the liquid electrolyte and maybe from residual DMF solution, the peak at 1735 cm^{-1} gets stronger in intensity and shifts towards bigger wavenumbers as the PEG amount increases. This could be due to the direct proportion between the PEG amount and the absorbed liquid electrolyte in the samples that explained by the micropore-forming property of the PEG [81]. The peak at 2242 cm^{-1} for nitrile group of PAN only changes for the sample S4 by giving a peak at 2244 cm^{-1}. The peak at 3477 cm^{-1}, related with N-H stretching, is observed to shift to 3467 cm^{-1}. Apart from that, all the peaks for N-H stretching of the wet samples at each composition are lower in intensity than their dry corresponding versions given in Figure 4.1. It implies better interaction between PAN and PEG in the liquid electrolyte presence, and also the interactions between the polymers and the liquid electrolyte.

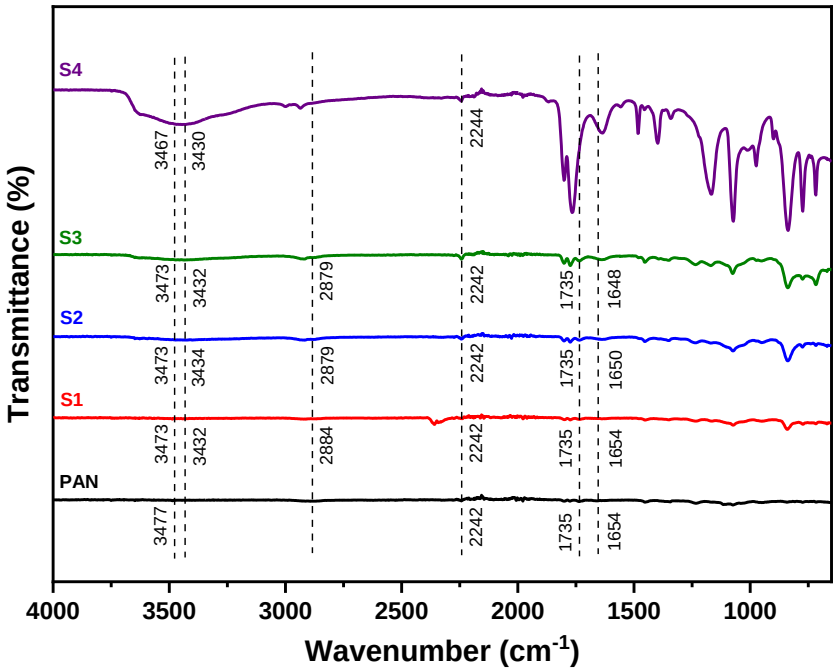

Figure 4.2 : FTIR spectra of the polymer electrolytes PAN, S1, S2, S3 and S4.

The characteristic O-H stretching vibration of PEG, which is at 1279 cm^{-1} for pure PEG, is not seen for the samples S3 and S4 signifying complexations between Li^+ ions and PEG [78]. One of the characteristic peaks of $LiPF_6$ normally seen at around 1267 cm^{-1} does not appear for any of the samples that may arise from complexations between the ions and polymers, mostly PAN as it exists in all the samples. A different peak of $LiPF_6$ at 1654 cm^{-1} for wet PAN sample moves towards lower wavenumber side as PEG content increases and completely disappears for the sample S4. This represents another complexation between the salt and S4 [82].

4.1.2 TG and DSC analysis of the gel polymer electrolytes

TG and DSC were applied to the samples to determine their thermal stability which is an essential aspect for safe usage in their practical applications. The weight change through heating of the dry polymer samples with varying compositions of PAN and PEG and the wet versions of these samples containing the liquid electrolyte are represented in Figure 4.3. For the dry samples, the initial mass loss for each sample is considered to belong to the moisture. After this region, the reactions of PAN, i.e. nitrile groups' cyclization, dehydrogenation and oxidation, take place, and the samples start to lose mass. The first major loss for PAN sample starts at around 328.6 °C which is its decomposition temperature. The decomposition of the PEG is also in this region causing the two phased degradation steps for the blended samples. The dry PAN sample has the highest decomposition temperature, though, sample S4 has the highest residual weight % of 44.9 at the end of the process. It implies better integration of the constituents in S4 as the final residual weight of the S1, S2 and S3 is less. Last step for the mass loss is related to the carbonation process of PAN which is given until 600 °C [64, 75, 83, 84].

For the electrolyte samples, the first significant loss starts at 63.3 °C for PAN, 60.6 °C for S1, 61.6 °C for S2, 64.5 °C for S3 and 60.9 °C for S4. These reductions in the early stages of the plots are caused by the moisture and the evaporation of the volatile organic compounds, i.e. EC, DEC and DMC [72]. The polymer-based decompositions start at the further temperature levels between 306°C and 339 °C. The highest decomposition temperature belongs to S1 but the highest mass loss through heating is for S3.

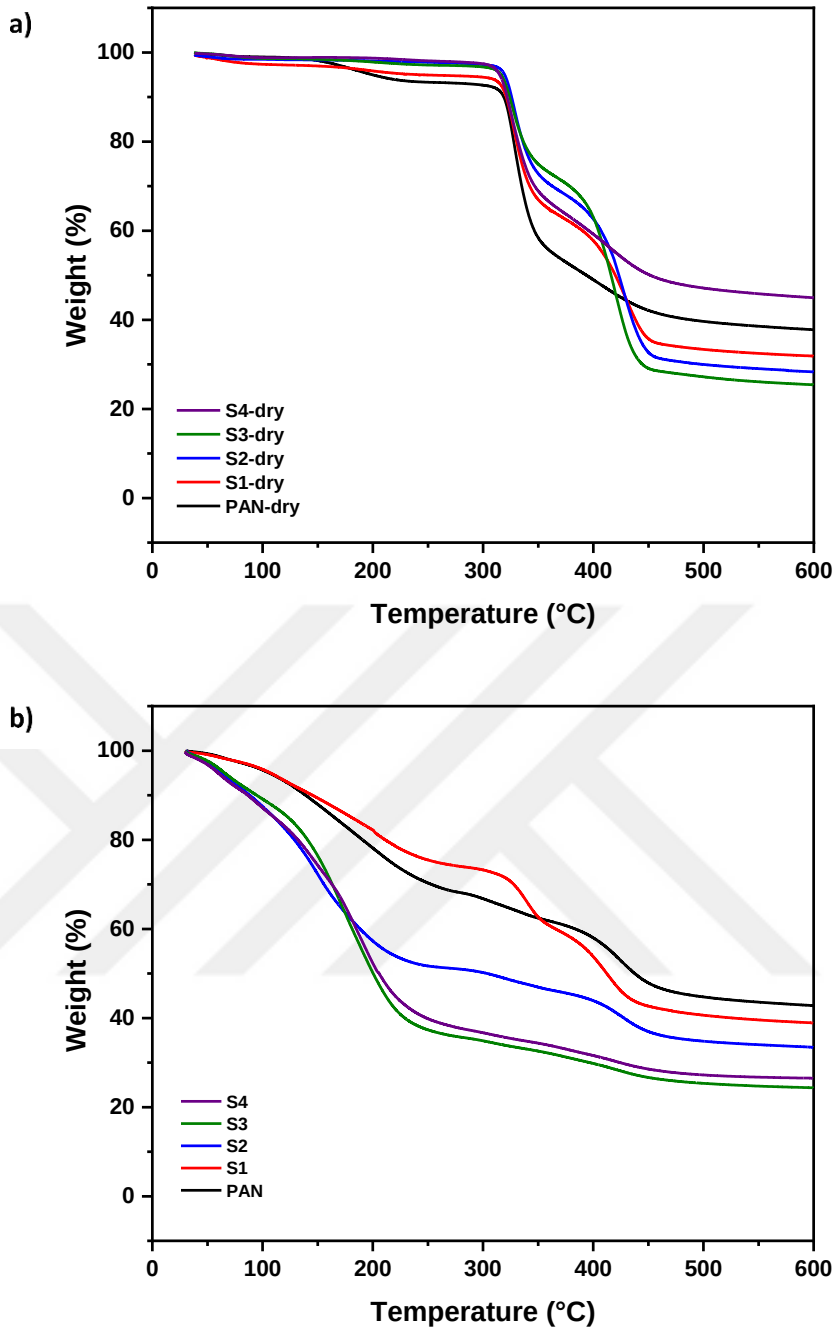

Figure 4.3 : TG curves of a) dry polymer samples and b) polymer electrolyte samples for PAN, S1, S2, S3 and S4.

Independent of the plasticizer ratio, all the wet samples have decomposition temperature (T_d) values which are smaller than those of their dry corresponding except the sample S1. The T_d and final residual weight percentage (W_f) of the samples are tabulated in Table 4.2 below.

Table 4.2 : T_d and W_f values for the polymer samples with varying compositions of PAN and PEG.

Sample	T_d (°C)	W_f (%)
PAN-dry	328.6	37.7
S1-dry	327.6	31.8
S2-dry	328.5	28.2
S3-dry	326.2	25.4
S4-dry	325.6	44.9
PAN	306.2	42.7
S1	339.8	38.9
S2	318.8	33.4
S3	307.4	24.3
S4	306.6	26.5

The DSC thermograms of PAN, S1, S2, S3 and S4 are given in Figure 4.4 and Figure 4.5 for the dry and wet versions of the samples, respectively. The indicated exothermic peaks are at around the decomposition temperatures of each of the samples within the region where the major mass loss occur.

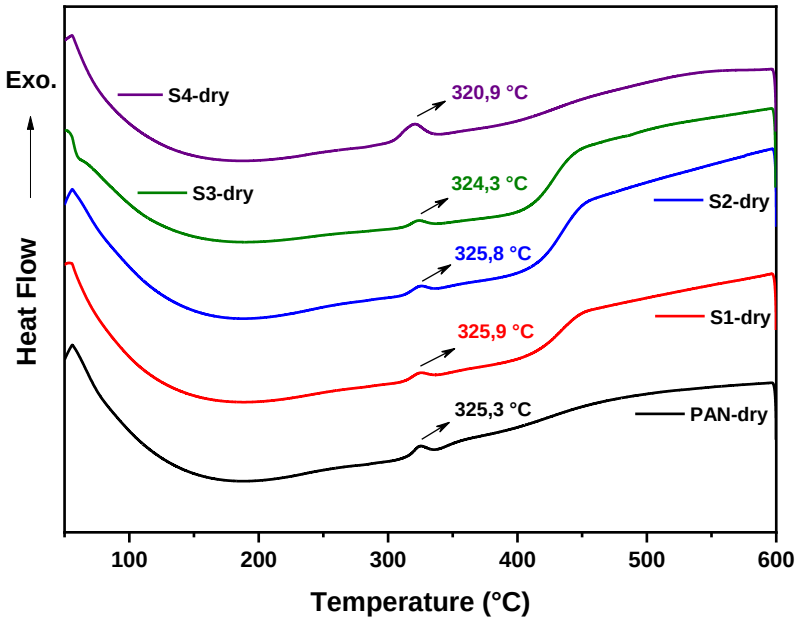

Figure 4.4 : DSC curves for dry polymer samples of PAN, S1, S2, S3 and S4.

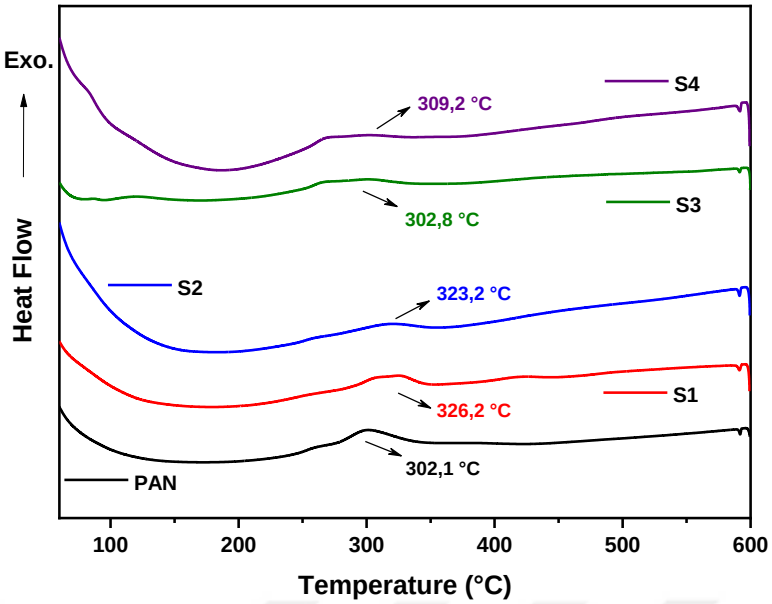

Figure 4.5 : DSC curves for polymer electrolyte samples of PAN, S1, S2, S3 and S4.

It is seen that inclusion of the liquid electrolyte lowers the temperature for these peaks except for the sample S1 that is coherent with the thermally stable profile of it in Figure 4.3b. T_g values of the samples were determined by the first derivative of the heat flow plot and given in Figure 4.6 and Figure 4.7. The endothermic peaks in the thermograms show the T_g values for each sample. The T_g values are mostly lower than that of PAN in Figure 4.6 as a result of the addition of the plasticizer PEG.

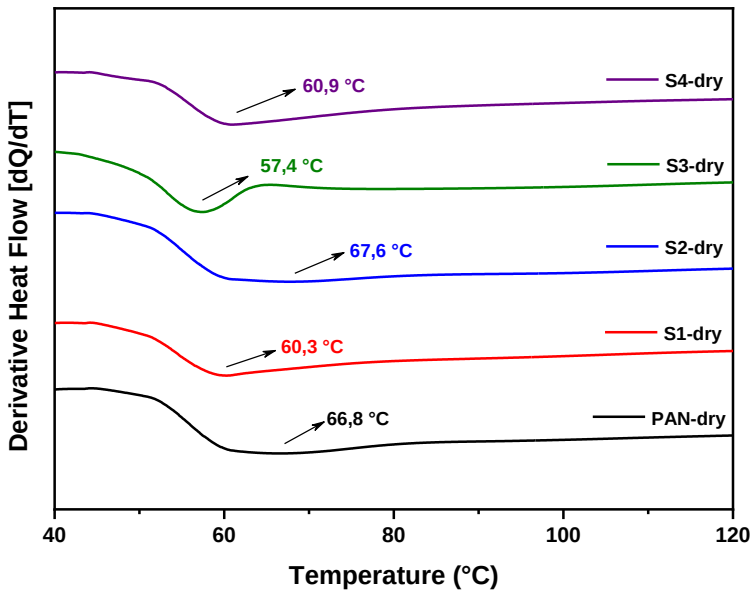

Figure 4.6 : The first derivatives of the DSC curves for dry polymer samples of PAN, S1, S2, S3 and S4 in the range of 40-120 °C.

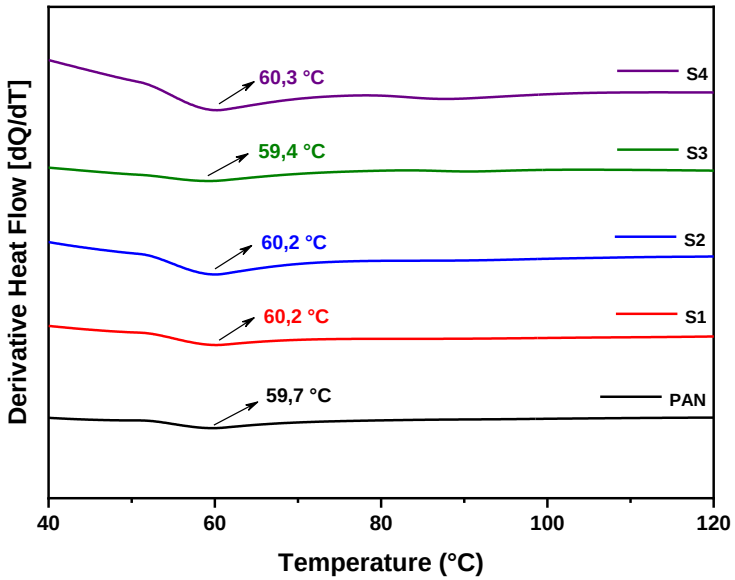

Figure 4.7 : The first derivatives of the DSC curves for polymer electrolyte samples of PAN, S1, S2, S3 and S4 in the range of 40-120 °C.

Moreover, except the sample S3, the samples exhibit the glass-transition at decreased temperatures when they absorb the liquid electrolyte. The temperature (T_{peak}) and heat flow (Q_{peak}) values of the exothermic peaks and also T_g values for the samples are given in following Table 4.3.

Table 4.3 : T_{peak}, Q_{peak} and T_g values for the polymer samples with varying compositions of PAN and PEG.

Sample	T_{peak} (°C)	Q_{peak} (W/g)	T_g (°C)
PAN-dry	325.3	5.67	66.8
S1-dry	325.9	4.73	60.3
S2-dry	325.8	5.46	67.6
S3-dry	324.3	3.56	57.4
S4-dry	320.9	5.48	60.9
PAN	302.1	2.98	59.7
S1	326.2	2.93	60.2
S2	323.2	4.10	60.2
S3	302.8	3.41	59.4
S4	309.2	7.39	60.3

4.1.3 Ionic conductivity analysis of the gel polymer electrolytes

The room temperature ionic conductivity of PAN electrolyte and the gel polymer electrolytes with different compositions were studied by using the EIS technique. The Nyquist plots are given in Figure 4.8 with the inset showing the high-frequency region. The bulk resistance (R_b) obtained by using the equivalent circuit given in the figure, the thickness (l) that measured by a digital micrometer, and the calculated ionic conductivity (σ) values of the samples are given in Table 4.4.

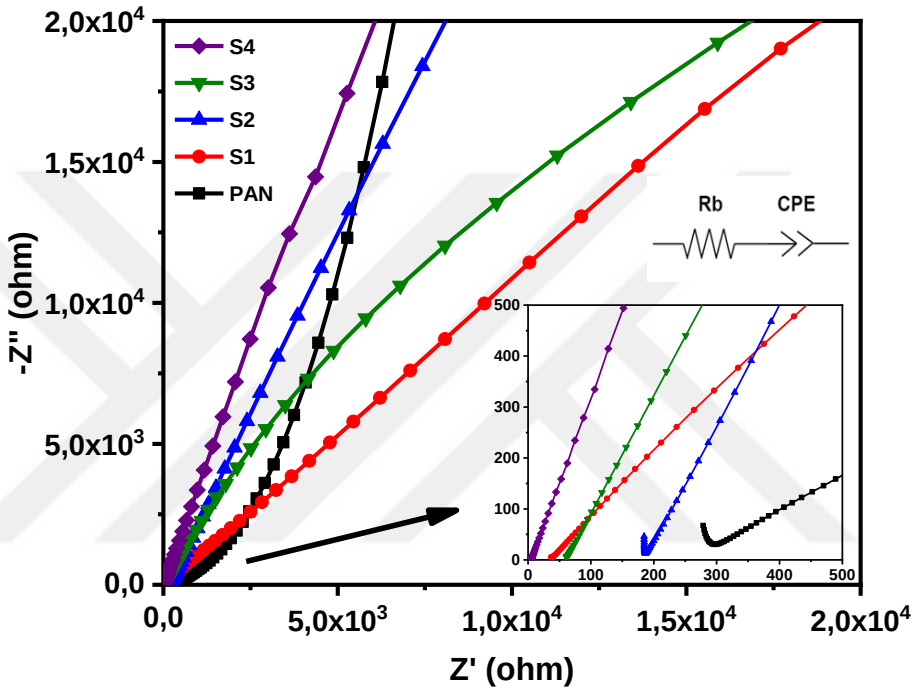

Figure 4.8 : AC impedance spectroscopy of the polymer electrolyte samples.

Table 4.4 : Calculation of the ionic conductivity of the polymer electrolyte samples PAN, S1, S2, S3 and S4.

Sample	R_b (ohm)	l (cm)	σ (S/cm)
PAN	264.20	0.018	3.83×10^{-5}
S1	33.99	0.196	3.26×10^{-3}
S2	184.30	0.010	3.07×10^{-5}
S3	60.06	0.021	1.95×10^{-4}
S4	4.94	0.049	5.56×10^{-3}

The highest ionic conductivity value was obtained as 5.56×10^{-3} S/cm with the sample S4. Although there is no direct relation between the ionic conductivity and the increased PEG ratio, the sample S4 has a value that is comparable with that of the liquid electrolytes.

4.1.4 Li-ion transference number analysis of the gel polymer electrolytes

Li^+ transference number measurements are plotted for PAN electrolyte and the gel polymer electrolytes in Figure 4.9 below.

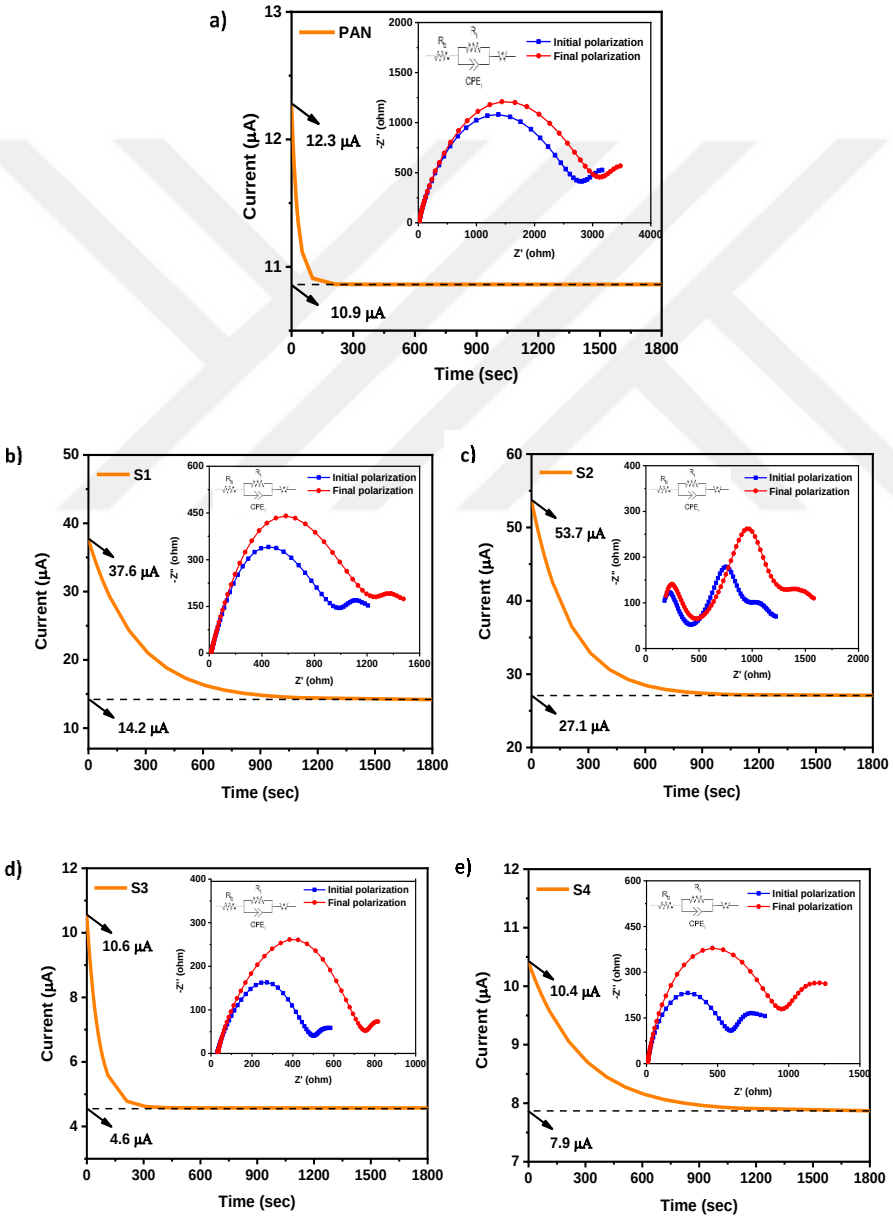

Figure 4.9 : Chronoamperometry curves by 10 mV DC polarization with inset AC EIS plots of the polymer electrolyte samples: a) PAN, b) S1, c) S2, d) S3 and e) S4.

The insets demonstrate the Nyquist plots of the impedance measurements obtained before and after the chronoamperometry. The transference numbers and all the parameters necessary for the calculations are given in Table 4.5.

Table 4.5 : The interfacial resistance, current and lithium-ion transference number of the polymer electrolyte samples PAN, S1, S2, S3 and S4.

Sample	$R_{i,0}$ (ohm)	$R_{i,ss}$ (ohm)	I_0 (μA)	I_{ss} (μA)	t_{Li}^+
PAN	2674	2990	12.3	10.9	0.89
S1	994.3	1257	37.6	14.2	0.79
S2	1384	2006	53.7	27.1	0.69
S3	468.8	724.5	10.6	4.6	0.65
S4	554.2	884	10.4	7.9	0.63

The value of t_{Li}^+ gradually decreases as the PEG ratio of the sample increases. Yet, all the electrolyte samples display outperformance considering most of the liquid electrolytes which have t_{Li}^+ <0.5 [72]. The importance of the higher transference number comes from the fact that it prevents nonhomogeneous and unstable ion deposition which may cause Li dendrites [73]. Another vital aspect of the high transference number values relates it with the charge/discharge stability, therefore it can be proposed that the increased t_{Li}^+ value will offer lower concentration polarization, better cycle stability and higher discharge capacity [59].

4.1.5 Electrochemical stability analysis of the gel polymer electrolytes

The LSV method was used to evaluate ESW of PAN electrolyte and the gel polymer electrolytes as shown in Figure 4.10. The breakdown point in each plot represented by a downward arrow indicates the sample decomposition and they are tabulated in Table 4.6.

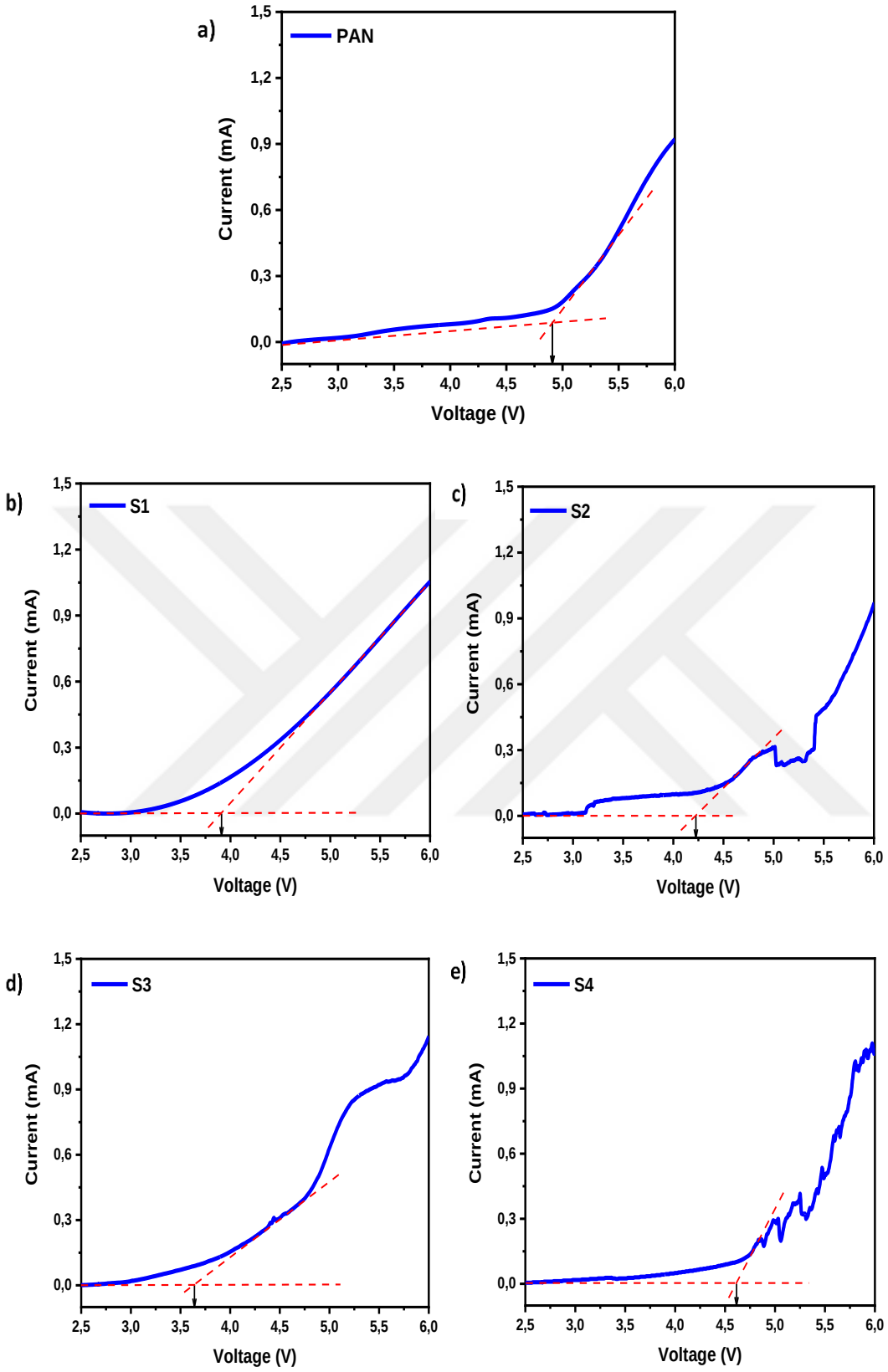

Figure 4.10 : LSV plots of the polymer electrolyte samples: a) PAN, b) S1, c) S2, d) S3 and e) S4.

Table 4.6 : Electrochemical stability window of the polymer electrolyte samples PAN, S1, S2, S3 and S4.

Sample	ESW (V)
PAN	4.91
S1	3.91
S2	4.23
S3	3.64
S4	4.62

The plasticizer addition to PAN impaired the materials respecting the electrochemical stability as expected [85]. However, a value between 4-5 V which obtained by the samples S2 and S4 is considered to be enough for a stable electrolyte [35]. Therefore, it can be concluded that the decomposition of a plasticized polymer electrolyte, i.e. gel polymer electrolyte, at a higher voltage value can be enabled with a proper sample composition.

4.2 Results for the Composite Gel Polymer Electrolytes

4.2.1 FTIR analysis of the composite gel polymer electrolytes

The structural effect of SiO_2 addition to the mixtures of PAN and PEG was evaluated via FTIR study. Figure 4.11 demonstrates the FTIR spectra for the composite gel polymer samples having PAN/PEG=2:1 (w/w) ratio and their corresponding electrolyte samples after the liquid electrolyte bathing.

In Figure 4.11a, the peak at 1233 cm^{-1} shifts to 1221 cm^{-1}. Moreover, the first C-H stretching peak relocates from 2874 cm^{-1} to 2850 cm^{-1}. In Figure 4.11b, O-H stretching of PEG does not demonstrate peak and the peak for C-H bending of CH for PAN is seen at a lower wavenumber for the electrolyte sample. The regions for C-H stretching of CH_2 of PAN and C-H stretching of PEG show the first peaks at 2875 cm^{-1} for the dry sample and 2850 cm^{-1} for the electrolyte sample. The C≡N stretching vibration keeps occurring in all the plots in Figure 4.11 while both the Si-O-H bending (at 800 cm^{-1} for C1-dry and at 805 cm^{-1} for C2-dry) and stretching (at 1096 cm^{-1} for both C1-dry and C2-dry) vibrations [86] disappear by the inclusion of the liquid electrolyte.

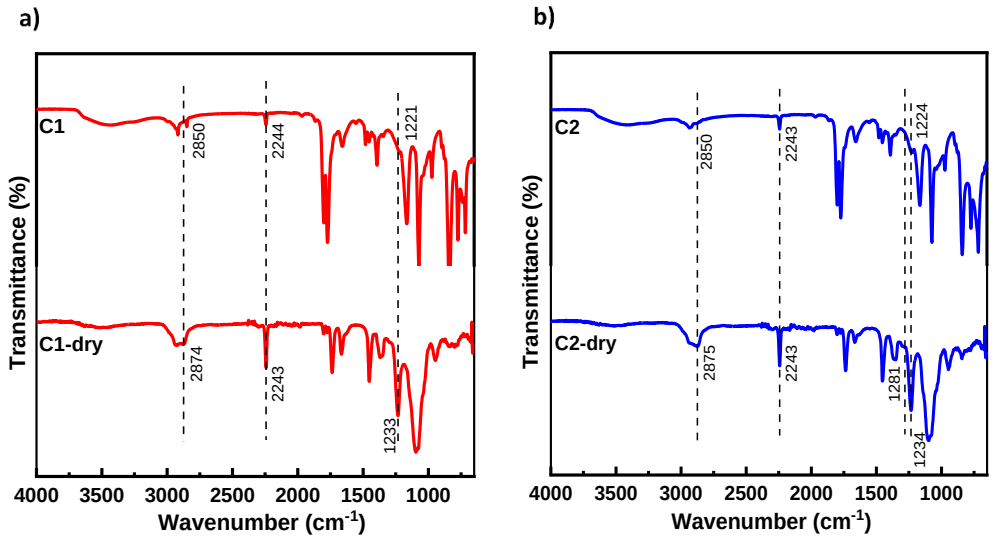

Figure 4.11 : FTIR spectra for the samples with PAN/PEG=2:1 (w/w): a) C1 and dry C1, and b) C2 and dry C2.

Contrary to the presence of the vibrational peaks for the O-H stretching and C-H bending of PEG in the electrolyte sample S2, these peaks do not appear in the composite electrolyte samples as shown in Figure 4.12. The C≡N stretching peaks change slightly and the minimum one belongs to C2. The C=O stretching gives multiple intensified peaks for C1 and C2. The elongated bands in the higher wavenumbers contain salt vibration peaks that implies better absorption of the liquid electrolyte as the silica content increases [82]. Besides, N-H stretching of PAN does not exist in the sample C1 while the O-H stretching of the PEG is not found in neither of the composite samples.

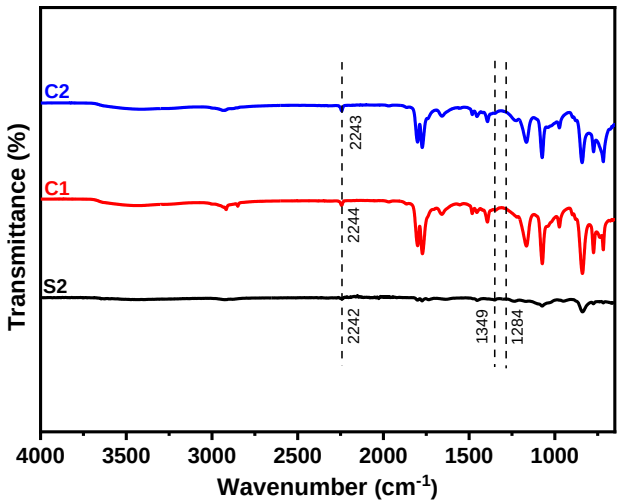

Figure 4.12 : FTIR spectra of the gel polymer electrolytes with different SiO_2 weight ratios for PAN/PEG=2:1 (w/w).

The vibrational peak for O-H stretching of PEG at 1280 cm^{-1} is not seen for C3 in Figure 4.13a. On the other hand, C-H stretching and bending peaks are present in C3 with lower intensities with respect to its dry corresponding, C3-dry. In Figure 4.13b, the vibrational peak of PAN assigned for C-H bending at 1232 cm^{-1} disappears in C4. Belonging to PEG, C-H stretching at 2884 cm^{-1} and O-H stretching at 1280 cm^{-1} also vanishes for C4.

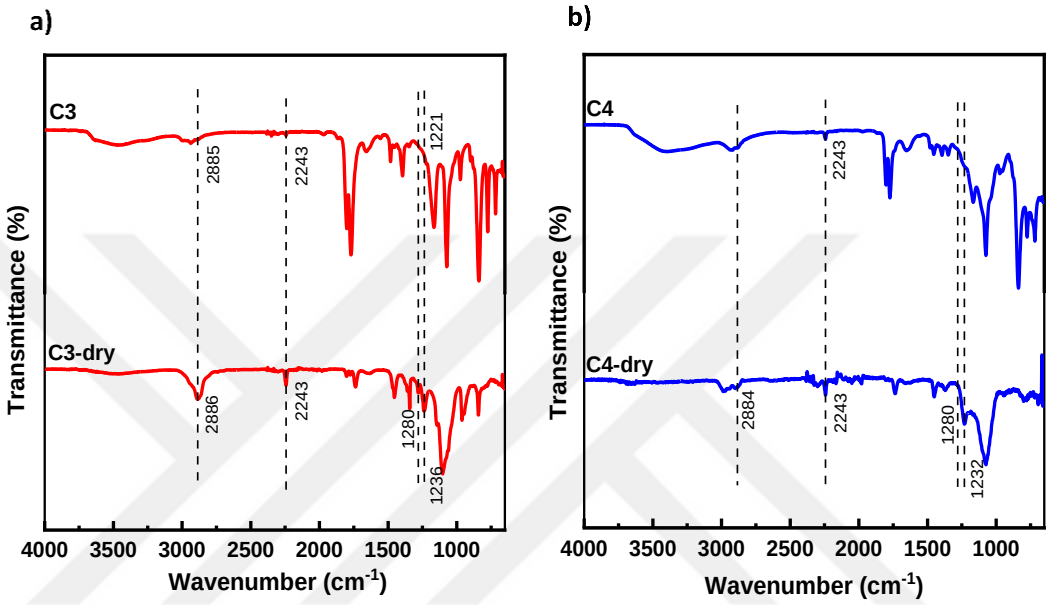

Figure 4.13 : FTIR spectra for the samples with PAN/PEG=1:1 (w/w): a) C3 and dry C3, and b) C4 and dry C4.

The multiple peaks seen between 1750-1800 cm^{-1} belong to the carbonyl stretching, and intensities are stronger for C3 and C4 samples due to their organic solvent contents. In the same way, the salt $LiPF_6$ in the liquid electrolyte causes the bands to elongate between 3000-3500 cm^{-1} [82]. The characteristic C≡N stretching vibration peak of PAN is seen at 2243 cm^{-1} in all the samples of Figure 4.13. Lastly, the Si-O-H stretching and bending peaks in C3-dry sample at 808 cm^{-1} and 1103 cm^{-1} [86], respectively, vanish in C3, C4-dry and C4.

As represented in Figure 4.14, the vibrational peak of C-H bending of PEG which is present in the sample S4 disappears for the composite samples of C3 and C4. The characteristic band of C-C stretching of PAN first loses peak intensity, and then gets stronger again with the increasing amount of silica. Among all the samples, C3 has the lowest intensity for C≡N stretching proving the best interaction between functional

nitrile group of PAN and silica. Similarly, the C=O stretching first decreases, and then increases in intensity with the addition of silica.

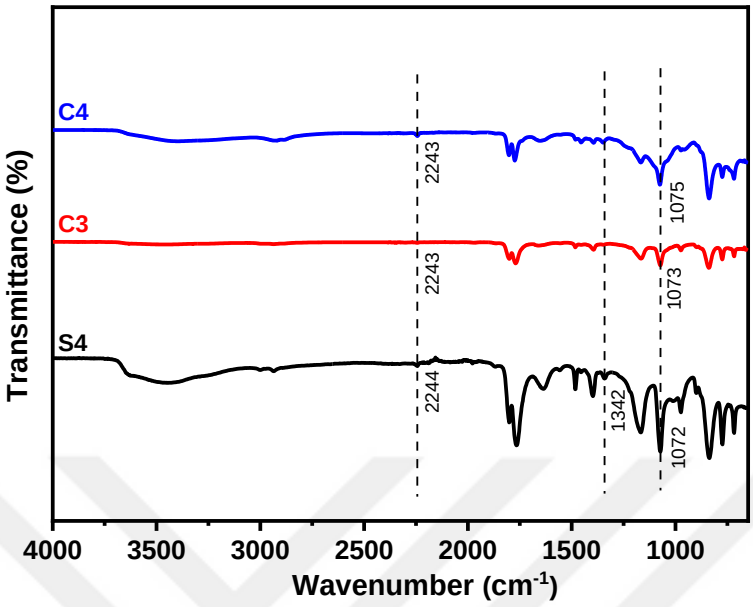

Figure 4.14 : FTIR spectra of the gel polymer electrolytes with different SiO_2 weight ratios for PAN/PEG=1:1 (w/w).

The peaks for N-H stretching of PAN at 3467 cm^{-1}, O-H stretching of PEG at 3430 cm^{-1} and for $LiPF_6$ salt at 3551 cm^{-1} found in S4, get lower intensities in C3 and completely vanish in C4. Also, the salt peak at 3604 cm^{-1} does not exist in the composite samples signifying good interaction between ions and polymer owing to the silica [82].

4.2.2 TG and DSC analysis of the composite gel polymer electrolytes

TG and DSC were applied to especially investigate the effect of filler material silica on the thermal stability of the composite polymer samples. In Figure 4.15, TG thermograms of the composite polymer samples are demonstrated in the temperature interval of 40-600 °C.

The C2 sample has the highest T_d value among the dry composite polymer samples shown in Figure 4.15a while the highest residual amount belongs to the sample C1. For a constant PAN/PEG weight ratio, the T_d value increases as the SiO_2 amount increases. Inversely, T_d value decreases with increasing amount of PEG for a constant SiO_2 ratio. The mass loss at the early stages of heating is considered directly related by the hydrophilic identity of the silica and the following vaporization of water [52].

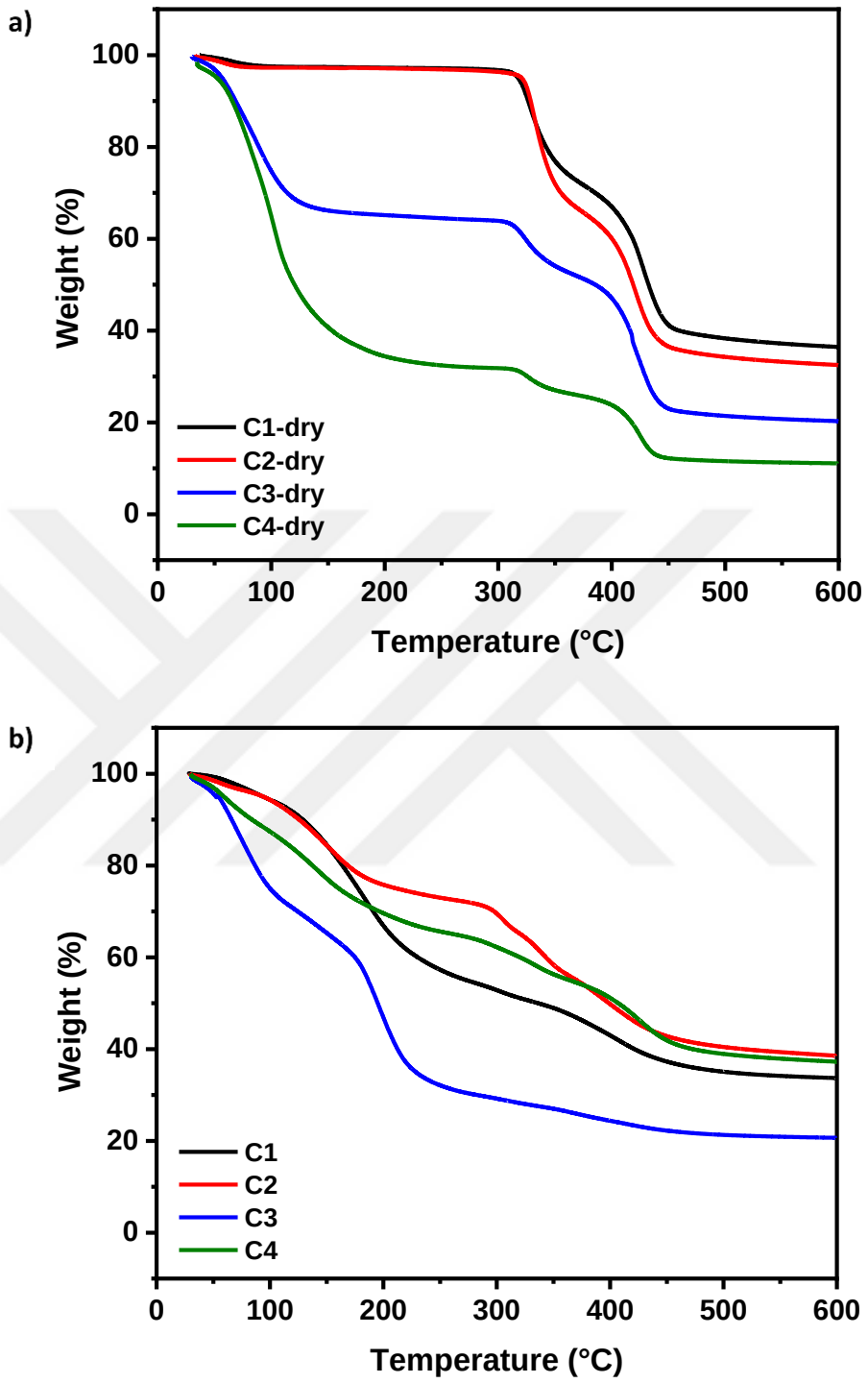

Figure 4.15 : TG curves of a) dry composite polymer samples and b) composite polymer electrolyte samples for C1, C2, C3 and C4.

For the composite gel polymer electrolytes of which the TG thermograms are given in Figure 4.15b, the T_d values are smaller than those of the dry samples and close to each other. The condition supplied by the relation between the ratio of the constituents for

dry composite samples is different for the composite electrolytes. There is not seen no direct relation for constant PEG or SiO_2 ratio. Yet, the sample C2 is the most thermally stable one with its T_d value of 305.9 °C. The initial mass loss especially for the samples C3 and C4 is caused by the liquid electrolyte, so the volatile organic solvent, retention capability of the samples that is enhanced by PEG. Table 4.7 gives all the T_d and W_f values of the composite polymer samples.

Table 4.7 : T_d and W_f values for the composite polymer samples with varying compositions of PAN, PEG and SiO_2.

Sample	T_d (°C)	W_f (%)
C1-dry	328.1	36.2
C2-dry	331.8	32.4
C3-dry	323.6	20.2
C4-dry	326.4	11.1
C1	302.1	33.6
C2	305.9	38.5
C3	305.6	20.6
C4	300.7	37.2

The DSC thermograms and indicated exothermic peaks of the composite polymer samples are represented in Figure 4.16. C2 turned out as the most stable sample for both its dry and electrolyte forms. Even though the order of stability (most stable to least stable) for the dry samples shows a resemblance between TG and DSC data, that order is nonidentical for the composite electrolyte samples. This condition once again originates due to the effect of the plasticizer and filler ratio in the samples.

The T_g values of the composite polymer samples are found by the first derivative plots of the DSC curves and shown in Figure 4.17. For all the plots, it is concluded that increasing the silica amount gives rise to higher T_g values, inferred from the endothermic peaks at the initial regions of the thermograms. The dry sample of C3 with the highest plasticizer and the lowest filler ratio has the smallest T_g value. However, the liquid electrolyte bath affects the situation, and for the electrolyte

samples it is seen that sample C1 has the smallest T_g value. T_{peak}, Q_{peak} and T_g values from the DSC curves for the composite gel polymer samples are listed in Table 4.8.

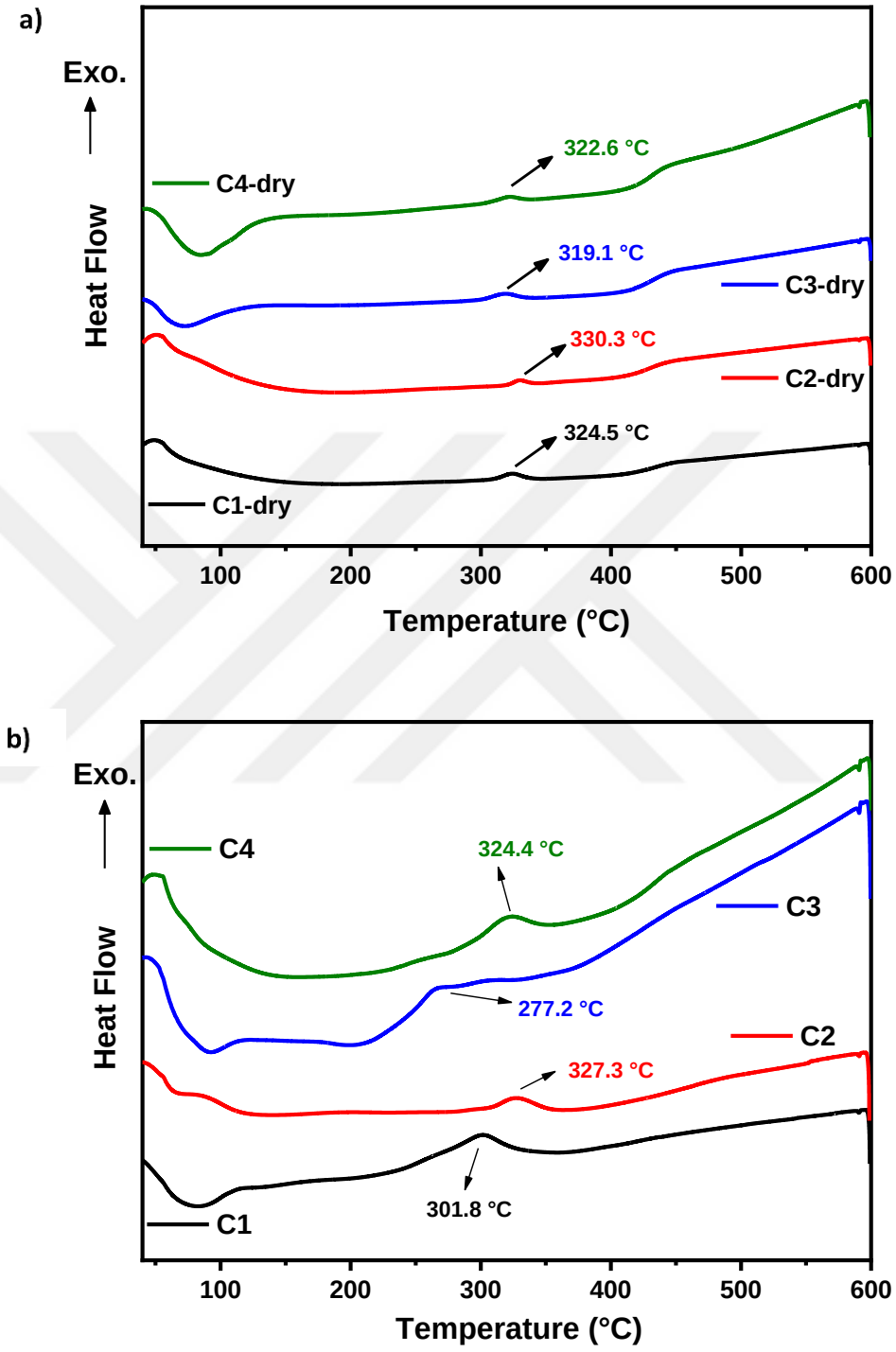

Figure 4.16 : DSC curves of a) dry composite polymer samples and b) composite polymer electrolyte samples for C1, C2, C3 and C4.

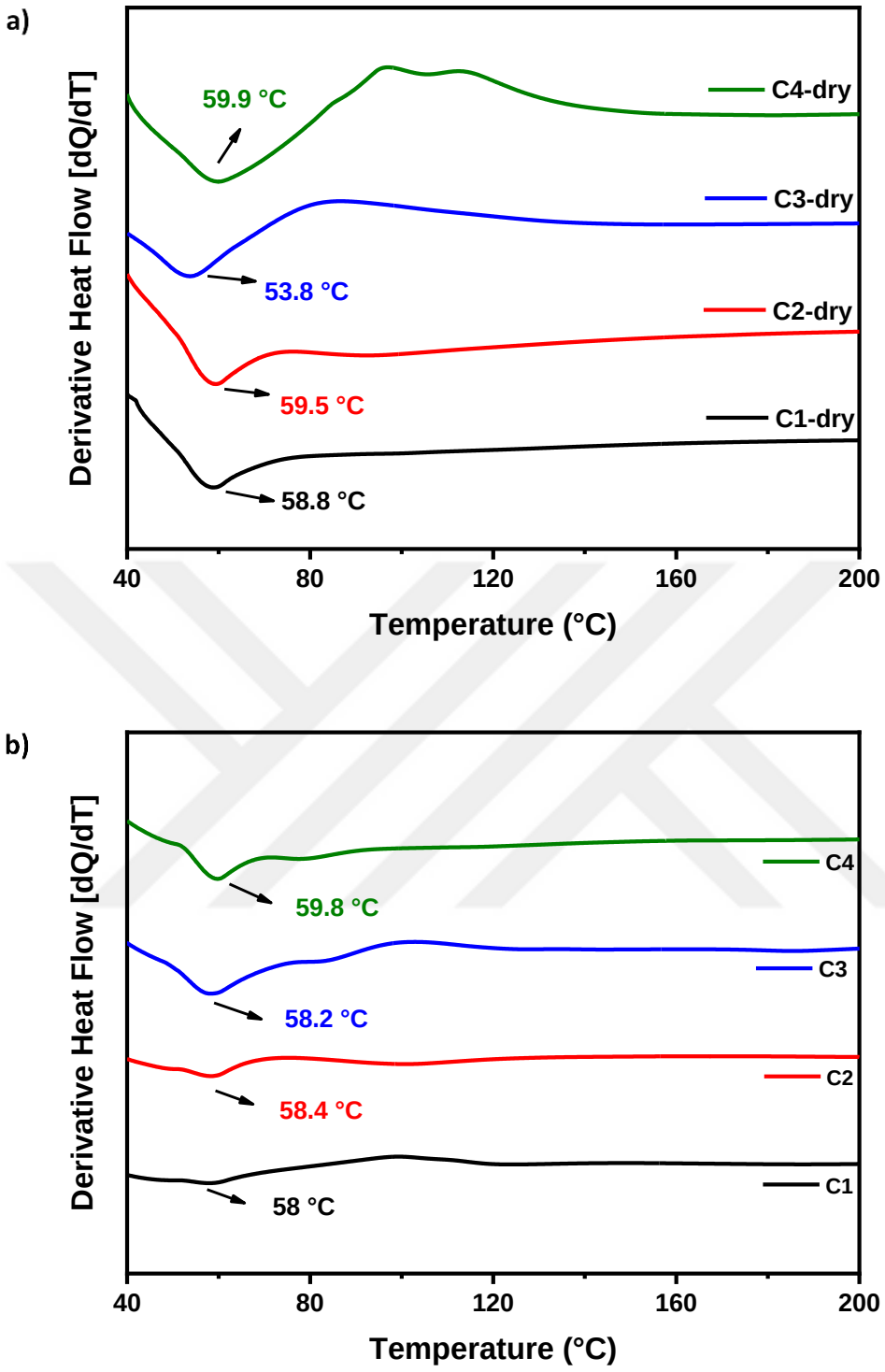

Figure 4.17 : The first derivatives of the DSC curves of a) dry composite polymer samples and b) composite polymer electrolyte samples for C1, C2, C3 and C4 in the range of 40-200 °C.

Table 4.8 : T_{peak}, Q_{peak} and T_g values for the composite polymer samples with varying compositions of PAN, PEG and SiO_2.

Sample	T_{peak} (°C)	Q_{peak} (W/g)	T_g (°C)
C1-dry	324.5	2.08	58.8
C2-dry	330.3	2.68	59.5
C3-dry	319.1	2.14	53.8
C4-dry	322.6	3.33	59.9
C1	301.8	1.82	58
C2	327.3	0.53	58.4
C3	277.2	2.70	58.2
C4	324.4	2.96	59.8

4.2.3 Ionic conductivity analysis of the composite gel polymer electrolytes

The ionic conductivity values of the composite gel polymer electrolyte samples at room temperature were evaluated via Nyquist plots. The plots with the equivalent circuit which was used for fitting and tabulated data for the calculation are given in Figure 4.18 and Table 4.9 below, respectively.

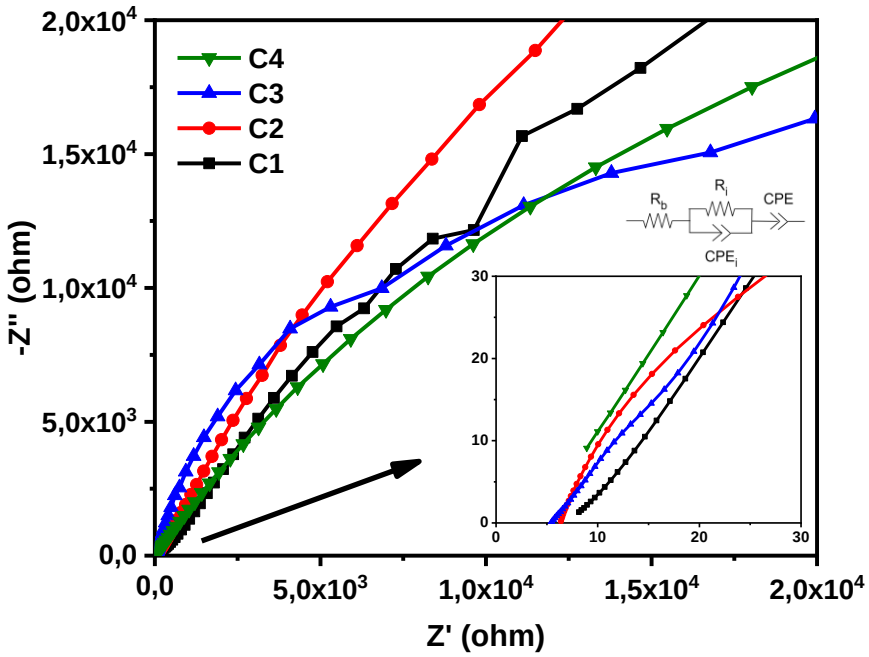

Figure 4.18 : AC impedance spectroscopy of the composite gel polymer electrolytes.

Table 4.9 : Calculation of the ionic conductivity of the composite gel polymer electrolytes.

Sample	R_b (ohm)	l (cm)	σ (S/cm)
C1	6.50	0.019	1.68×10^{-3}
C2	6.04	0.020	1.85×10^{-3}
C3	3.87	0.039	5.70×10^{-3}
C4	2.37	0.029	7.00×10^{-3}

It is concluded that the ionic conductivity increases with the increasing SiO_2 amount provided that the PAN:PEG ratio is constant, e.g. C1 to C2 and C3 to C4. Additionally, the improvement is more explicit with the increasing amount of PEG in the case of constant PAN:SiO_2 ratio, e.g. C1 to C3 and C2 to C4. As a result, sample C4 having the highest ratio of PEG and SiO_2 also has the highest value of ionic conductivity.

4.2.4 Li-ion transference number analysis of the composite gel polymer electrolytes

The transference number evaluation was done by the method as it is for the gel polymer electrolytes. The Nyquist and chronoamperometry curves for each composite gel polymer electrolytes are demonstrated as in Figure 4.19 and Figure 4.20.

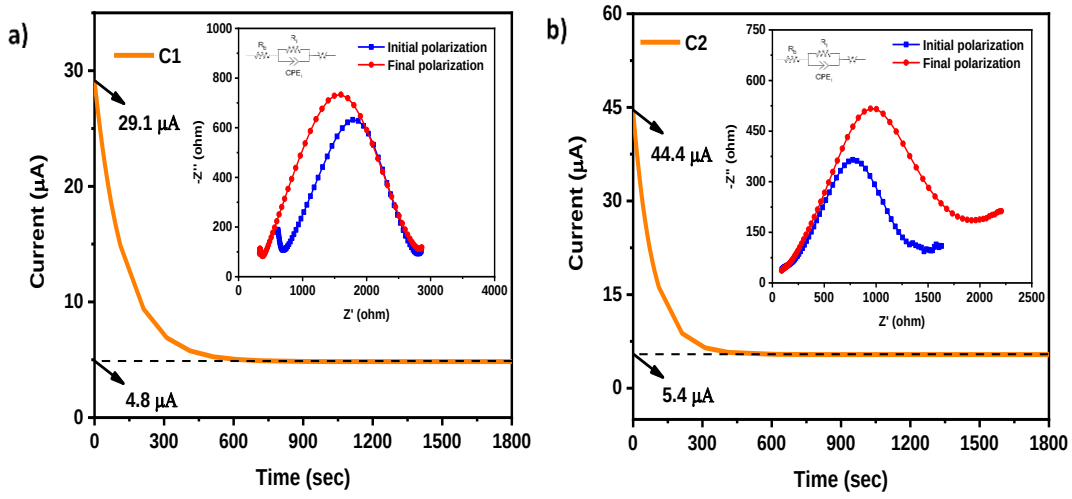

Figure 4.19 : Chronoamperometry curves by 10 mV DC polarization with inset AC EIS plots of the composite gel polymer electrolytes: a) C1 and b) C2.

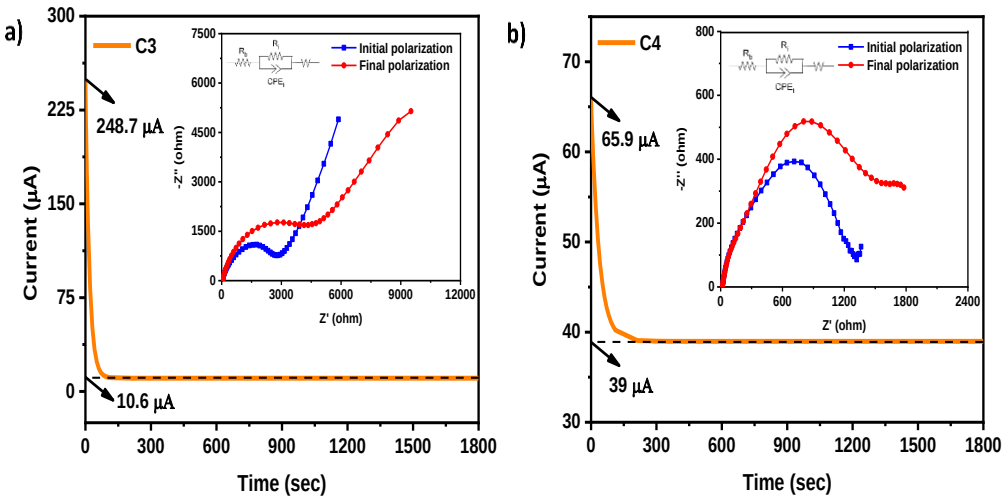

Figure 4.20 : Chronoamperometry curves by 10 mV DC polarization with inset AC EIS plots of the composite gel polymer electrolytes: a) C3 and b) C4.

All the composite gel polymer electrolytes yielded moderate to high t_{Li}^{+} values. In spite of the relatively low ionic conductivity value, the sample C1 has the highest transference number among the composite electrolytes. This arises from a better interaction at the interface between the electrolyte, i.e. C1, and the electrode, i.e. lithium foil [87]. Table 4.10 lists the measured resistance and current values based on AC impedance and DC polarization methods together with the calculated transference number of the composite gel polymer electrolytes.

Table 4.10 : Calculation of the lithium-ion transference number of the composite gel polymer electrolytes C1, C2, C3 and C4.

Sample	$R_{i,0}$ (ohm)	$R_{i,ss}$ (ohm)	I_0 (µA)	I_{ss} (µA)	t_{Li}^{+}
C1	2322	2610	29.1	4.8	0.89
C2	1697	2335	44.4	5.4	0.73
C3	2296	3855	248.7	10.6	0.60
C4	1300	1722	65.9	39	0.75

4.2.5 Electrochemical stability analysis of the composite gel polymer electrolytes

The electrochemical stability window, determined via LSV method and showing the oxidative stability, of the composite gel polymer electrolyte samples is presented in the following Figure 4.21. The downward arrows point out the breakdown point of the samples and those are given in Table 4.11.

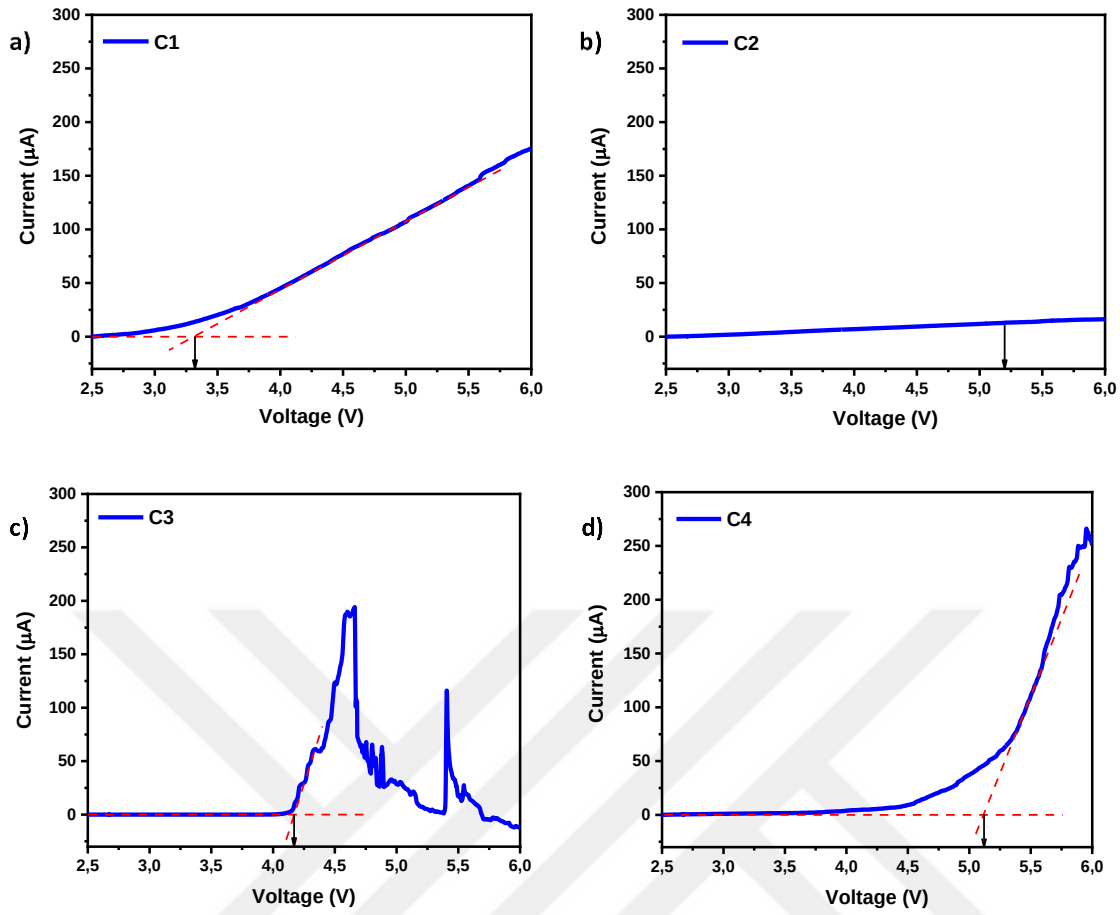

Figure 4.21 : LSV plots of the composite gel polymer electrolytes: a) C1, b) C2, c) C3 and d) C4.

In the study, increasing the SiO_2 proportion in the electrolyte returned as elevated electrochemical stability. Sample C1 has a relatively low electrochemical stability and it can be associated with its low ionic conductivity value with respect to those of the other composite electrolytes, i.e. C2, C3 and C4 [67]. Moreover, samples C2 and C4 can be anticipated electrolytes for the practical battery application owing to their high oxidative decompositions exceeding 5V.

Table 4.11 : Electrochemical stability window of the composite gel polymer electrolytes C1, C2, C3 and C4.

Sample	ESW (V)
C1	3.32
C2	5.20
C3	4.17
C4	5.12

4.2.6 Half-cell performance analysis of the composite gel polymer electrolytes

Based on the previous characterization results, especially those for the electrochemical stability window, the electrolytes C2 and C4 were found to be proper to be used in the charge/discharge cycle test. Half-cells with the Li//C2//LCO and Li//C4//LCO arrangements were subjected to cycling at constant current and at 0.1C rate. Charging and discharging specific capacity for the cells are measured and represented as in Figure 4.22.

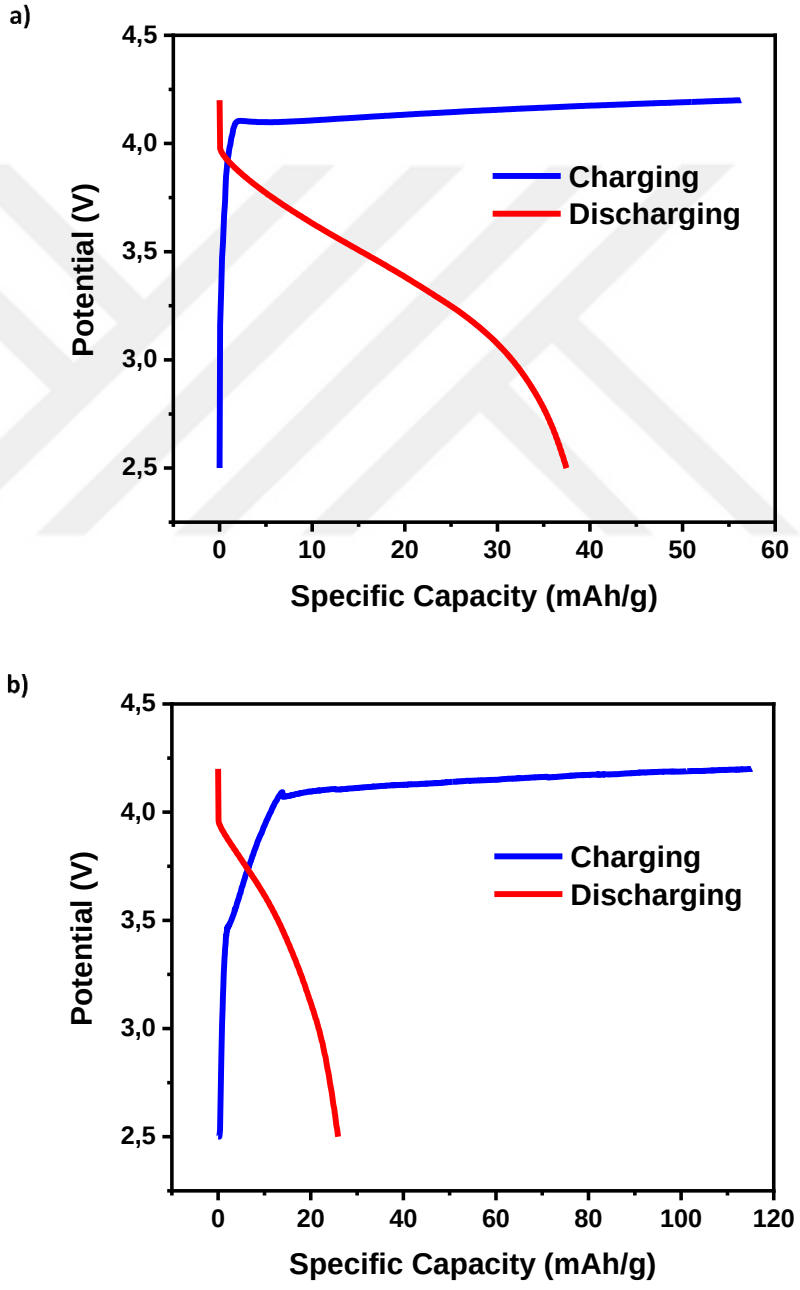

Figure 4.22 : Galvanostatic charge and discharge profile for the first cycle of the half-cells with the electrolyte samples: a) C2 and b) C4.

By the curves, the charging and discharging capacity of C2 were estimated as 56.3 mAh/g and 37.5 mAh/g, respectively. Also, 115.3 mAh/g of charging capacity and 25.9 mAh/g of discharging capacity were obtained for C4. Although the charging capacity of C4 nearly doubles that of C2, the gap between the charging and discharging profiles is smaller for C2. The former can be associated with the high ionic conductivity of C4 while electrochemical stability, i.e. low polarization, of C2 can be the reason behind the latter [87].

5. CONCLUSIONS AND RECOMMENDATIONS

Recently, the electrolytes in the form of quasi-solid or gel structures are being extensively studied as they represent an intermediate stage between liquid and all-solid electrolytes. In this study, gel polymer/composite gel polymer electrolytes were prepared and characterized for battery applications. The PAN-based electrolyte systems with varying concentrations of PEG plasticizer and SiO_2 nanofiller were obtained via solution casting and following immersion into the liquid electrolyte of $LiPF_6$ in EC/DEC/DMC. The structural and thermal properties of the samples were studied by FTIR spectroscopy and TG/DSC method, respectively. Moreover, the electrolytes were compared in terms of their electrochemical properties of ionic conductivity, Li^+ ion transference number and electrochemical stability. Lastly, the initial charge/discharge capacity of the fabricated half-cells with two different composite gel polymer electrolytes were investigated.

FTIR study revealed that there is interaction between the components within the electrolytes. Also, it was seen that the plasticizer and the nanofiller addition to the samples increase the absorption of the liquid electrolyte. Thermal analysis yielded a decomposition temperature of more than 300 °C for all the electrolytes without any distinguished positive effect of nanofiller on the thermal stability. The samples S1 with 339.8 °C and C2 with 305.9 °C have the highest T_d values among the gel polymer and composite gel polymer electrolytes, respectively.

It was displayed that it is possible to obtain ionic conductivity values close to those of the conventional liquid electrolytes (~10^{-3} S/cm), with gel/composite gel polymer electrolytes such that sample S4 has 5.56×10^{-3} S/cm and sample C4 has 7.00×10^{-3} S/cm of room temperature ionic conductivity. Furthermore, as the plasticizer ratio was increased transference number kept its decline for the gel polymer electrolytes. PAN electrolyte has a value of 0.89 while the transference number of the sample S4, having the highest PEG ratio, is 0.63. There is no such relation between t_{Li^+} values and nanosilica ratio for the composite gel polymer electrolytes, though the sample C1 exhibited a superior value of 0.89.

Besides, sample S4 kept its oxidative stability up to 4.62 V while samples C2 and C4 showed their electrochemical decompositions over 5 V. Ultimately, a battery study was conducted for half-cells with the composite gel polymer electrolytes of C2 and C4 as they were found to be favorable. The performance of the cells was evaluated based on the high charging capacity of C4 and the better charge/discharge efficiency of C2. However, relatively low values of the discharge capacity of the cells imply the necessity for further work that would be particularly on the cycled cells.

In conclusion, gel polymer electrolytes with certain preparation methods, materials and compositions were reported as possible candidates to be used in electrochemical battery cells. Further study would be on expanding the battery cycling test inclusively presenting the trend for multiple consecutive charge/discharge cycles and improving the discharge capacity, on preparing composite gel polymer electrolytes with different ratios of nanosilica, on applying different filler material, on eliminating the organic solvents via individual inclusion of the salt, on carrying out ionic conductivity test under varying temperature levels, and on using a different preparation method which allows the polymer matrix to have controlled pore structure so as to observe physicochemical properties of the electrolytes.

REFERENCES

[1] **IEA.** (2022). World energy outlook 2022. Paris, France: IEA. Retrieved from https://www.iea.org/reports/world-energy-outlook-2022

[2] **Guney, M. S., & Tepe, Y.** (2017). Classification and assessment of energy storage systems. *Renewable and Sustainable Energy Reviews*, *75*, 1187-1197. https://doi.org/10.1016/j.rser.2016.11.102

[3] **Xiong, R., Pan, Y., Shen, W., Li, H., & Sun, F.** (2020). Lithium-ion battery aging mechanisms and diagnosis method for automotive applications: Recent advances and perspectives. *Renewable and Sustainable Energy Reviews*, *131*, 110048. https://doi.org/10.1016/j.rser.2020.110048

[4] **Sehrawat, P., Julien, C., & Islam, S. S.** (2016). Carbon nanotubes in Li-ion batteries: A review. *Materials Science and Engineering: B*, *213*, 12-40. https://doi.org/10.1016/j.mseb.2016.06.013

[5] **Fleischmann, J., Hanicke, M., Horetsky, E., Ibrahim, D., Jautelat, S., Linder, M., ... & van de Rijt, A.** (2023). Battery 2030: Resilient, sustainable, and circular. *McKinsey & Company*, 2-18. Retrieved from https://www.mckinsey.com/industries/automotive-and-assembly/our-insights/battery-2030-resilient-sustainable-and-circular

[6] **Manthiram, A.** (2017). An outlook on lithium ion battery technology. *ACS central science*, *3*(10), 1063-1069. https://doi.org/10.1021/acscentsci.7b00288

[7] **Watanabe, T., Inafune, Y., Tanaka, M., Mochizuki, Y., Matsumoto, F., & Kawakami, H.** (2019). Development of all-solid-state battery based on lithium ion conductive polymer nanofiber framework. *Journal of Power Sources*, *423*, 255-262. https://doi.org/10.1016/j.jpowsour.2019.03.066

[8] **Fan, L. Z., He, H., & Nan, C. W.** (2021). Tailoring inorganic–polymer composites for the mass production of solid-state batteries. *Nature Reviews Materials*, *6*(11), 1003-1019. https://doi.org/10.1038/s41578-021-00320-0

[9] **Url-1** <https://www.quantumscape.com/blog/solid-state-battery-landscape/>, date retrieved 15.10.2023.

[10] **Goodenough, J. B.** (2013). Evolution of strategies for modern rechargeable batteries. *Accounts of chemical research*, *46*(5), 1053-1061. https://doi.org/10.1021/ar2002705

[11] **Liang, S., Yan, W., Wu, X., Zhang, Y., Zhu, Y., Wang, H., & Wu, Y.** (2018). Gel polymer electrolytes for lithium ion batteries: Fabrication, characterization and performance. *Solid State Ionics*, *318*, 2-18. https://doi.org/10.1016/j.ssi.2017.12.023

[12] **Pistoia, G.** (2005). Primary Batteries. In *Batteries for Portable Devices* (pp. 33–76). https://doi.org/10.1016/B978-044451672-5/50004-1

[13] **Pistoia, G.** (2005). Rechargeable Batteries. In *Batteries for Portable Devices* (pp, 77-145). https://doi.org/10.1016/B978-044451672-5/50005-3

[14] **Arya, A., & Sharma, A. L.** (2020). A glimpse on all-solid-state Li-ion battery (ASSLIB) performance based on novel solid polymer electrolytes: a topical review. *Journal of Materials Science*, *55*(15), 6242-6304. https://doi.org/10.1007/s10853-020-04434-8

[15] **Liang, Y., Zhao, C. Z., Yuan, H., Chen, Y., Zhang, W., Huang, J. Q., ... & Zhang, Q.** (2019). A review of rechargeable batteries for portable electronic devices. *InfoMat*, *1*(1), 6-32. https://doi.org/10.1002/inf2.12000

[16] **Kularatna, N., & Gunawardane, K.** (2021). Rechargeable battery technologies: An electronic circuit designer's viewpoint. In *Energy Storage Devices for Renewable Energy-Based Systems* (pp. 65–98). https://doi.org/10.1016/B978-0-12-820778-9.00001-2

[17] **Wang, S., Fan, Y., Stroe, D.-I., Fernandez, C., Yu, C., Cao, W., & Chen, Z.** (2021). Lithium-ion battery characteristics and applications. In *Battery System Modeling* (pp. 1–46). https://doi.org/10.1016/B978-0-323-90472-8.00003-2

[18] **DeMeuse, M. T.** (2021). Introduction to lithium-ion battery design. In *Polymer-Based Separators for Lithium-Ion Batteries* (pp. 1–19). https://doi.org/10.1016/B978-0-12-820120-6.00002-7

[19] **Fichtner, M., Edström, K., Ayerbe, E., Berecibar, M., Bhowmik, A., Castelli, I. E., ... & Weil, M.** (2022). Rechargeable batteries of the future—the state of the art from a BATTERY 2030+ perspective. *Advanced Energy Materials*, *12*(17), 2102904. https://doi.org/10.1002/aenm.202102904

[20] **Wang, R., Cui, W., Chu, F., & Wu, F.** (2020). Lithium metal anodes: Present and future. *Journal of Energy Chemistry*, *48*, 145-159. https://doi.org/10.1016/j.jechem.2019.12.024

[21] **Goodenough, J. B.** (2018). How we made the Li-ion rechargeable battery. *Nature Electronics*, *1*(3), 204-204. https://doi.org/10.1038/s41928-018-0048-6

[22] **Nzereogu, P. U., Omah, A. D., Ezema, F. I., Iwuoha, E. I., & Nwanya, A. C.** (2022). Anode materials for lithium-ion batteries: A review. *Applied Surface Science Advances*, *9*, 100233. https://doi.org/10.1016/j.apsadv.2022.100233

[23] **Park J. K.** (2012). Introduction. In *Principles and Applications of Lithium Secondary Batteries* (pp. 1–7). https://doi.org/10.1002/9783527650408.ch1

[24] **Wang, Q., Jiang, L., Yu, Y., & Sun, J.** (2019). Progress of enhancing the safety of lithium ion battery from the electrolyte aspect. *Nano Energy*, *55*, 93-114. https://doi.org/10.1016/j.nanoen.2018.10.035

[25] **Kularatna, N., & Gunawardane, K.** (2021). Recent developments of high-performance battery systems. In *Energy Storage Devices for Renewable Energy-Based Systems* (pp. 173–180). https://doi.org/10.1016/B978-0-12-820778-9.00012-7

[26] **Liang, J., Luo, J., Sun, Q., Yang, X., Li, R., & Sun, X.** (2019). Recent progress on solid-state hybrid electrolytes for solid-state lithium batteries. *Energy Storage Materials, 21*, 308-334. https://doi.org/10.1016/j.ensm.2019.06.021

[27] **Zheng, F., Kotobuki, M., Song, S., Lai, M. O., & Lu, L.** (2018). Review on solid electrolytes for all-solid-state lithium-ion batteries. *Journal of Power Sources*, *389*, 198-213. https://doi.org/10.1016/j.jpowsour.2018.04.022

[28] **Huang, Y., Shao, B., & Han, F.** (2022). Solid-state batteries: an introduction. In *Solid State Batteries Volume 1: Emerging Materials and Applications* (pp. 1-20). American Chemical Society. https://doi.org/10.1021/bk-2022-1413.ch001

[29] **Li, C., Wang, Z. Y., He, Z. J., Li, Y. J., Mao, J., Dai, K. H., ... & Zheng, J. C.** (2021). An advance review of solid-state battery: Challenges, progress and prospects. *Sustainable Materials and Technologies*, *29*, e00297. https://doi.org/10.1016/j.susmat.2021.e00297

[30] **Agrawal, R. C., & Pandey, G. P.** (2008). Solid polymer electrolytes: materials designing and all-solid-state battery applications: an overview. *Journal of Physics D: Applied Physics*, *41*(22), 223001. https://doi.org/10.1088/0022-3727/41/22/223001

[31] **Yang, H., & Wu, N.** (2022). Ionic conductivity and ion transport mechanisms of solid-state lithium-ion battery electrolytes: A review. *Energy Science & Engineering*, *10*(5), 1643-1671. https://doi.org/10.1002/ese3.1163

[32] **Zheng, Y., Yao, Y., Ou, J., Li, M., Luo, D., Dou, H., ... & Chen, Z.** (2020). A review of composite solid-state electrolytes for lithium batteries: fundamentals, key materials and advanced structures. *Chemical Society Reviews*, *49*(23), 8790-8839. https://doi.org/10.1039/D0CS00305K

[33] **Manthiram, A., Yu, X., & Wang, S.** (2017). Lithium battery chemistries enabled by solid-state electrolytes. *Nature Reviews Materials*, *2*(4), 1-16. https://doi.org/10.1038/natrevmats.2016.103

[34] **Wu, Z., Xie, Z., Yoshida, A., Wang, Z., Hao, X., Abudula, A., & Guan, G.** (2019). Utmost limits of various solid electrolytes in all-solid-state lithium batteries: A critical review. *Renewable and Sustainable Energy Reviews*, *109*, 367-385. https://doi.org/10.1016/j.rser.2019.04.035

[35] **Wu, F., Zhang, K., Liu, Y., Gao, H., Bai, Y., Wang, X., & Wu, C.** (2020). Polymer electrolytes and interfaces toward solid-state batteries: Recent advances and prospects. *Energy Storage Materials*, *33*, 26-54. https://doi.org/10.1016/j.ensm.2020.08.002

[36] **Wang, L., Li, J., Lu, G., Li, W., Tao, Q., Shi, C., ... & Wang, S.** (2020). Fundamentals of electrolytes for solid-state batteries: challenges and perspectives. *Frontiers in Materials*, *7*, 111. https://doi.org/10.3389/fmats.2020.00111

[37] **Long, L., Wang, S., Xiao, M., & Meng, Y.** (2016). Polymer electrolytes for lithium polymer batteries. *Journal of Materials Chemistry A*, *4*(26), 10038-10069. https://doi.org/10.1039/C6TA02621D

[38] **Liu, W., Yi, C., Li, L., Liu, S., Gui, Q., Ba, D., ... & Liu, J.** (2021). Designing polymer-in-salt electrolyte and fully infiltrated 3D electrode for integrated solid-state lithium batteries. *Angewandte Chemie*, *133*(23), 13041-13050. https://doi.org/10.1002/ange.202101537

[39] **Yu, X., & Manthiram, A.** (2021). A review of composite polymer-ceramic electrolytes for lithium batteries. *Energy Storage Materials*, *34*, 282-300. https://doi.org/10.1016/j.ensm.2020.10.006

[40] **Tan, S. J., Zeng, X. X., Ma, Q., Wu, X. W., & Guo, Y. G.** (2018). Recent advancements in polymer-based composite electrolytes for rechargeable lithium batteries. *Electrochemical Energy Reviews*, *1*, 113-138. https://doi.org/10.1007/s41918-018-0011-2

[41] **Fu, X., Yu, D., Zhou, J., Li, S., Gao, X., Han, Y., ... & Wang, B.** (2016). Inorganic and organic hybrid solid electrolytes for lithium-ion batteries. *CrystEngComm*, *18*(23), 4236-4258. https://doi.org/10.1039/C6CE00171H

[42] **Meng, N., Zhu, X., & Lian, F.** (2022). Particles in composite polymer electrolyte for solid-state lithium batteries: A review. *Particuology*, *60*, 14-36. https://doi.org/10.1016/j.partic.2021.04.002

[43] **Ngai, K. S., Ramesh, S., Ramesh, K., & Juan, J. C.** (2016). A review of polymer electrolytes: fundamental, approaches and applications. *Ionics*, *22*, 1259-1279. https://doi.org/10.1007/s11581-016-1756-4

[44] **Hoang Huy, V. P., So, S., & Hur, J.** (2021). Inorganic fillers in composite gel polymer electrolytes for high-performance lithium and non-lithium polymer batteries. *Nanomaterials*, *11*(3), 614. https://doi.org/10.3390/nano11030614

[45] **Wang, S. H., Kuo, P. L., Hsieh, C. T., & Teng, H.** (2014). Design of poly (acrylonitrile)-based gel electrolytes for high-performance lithium ion batteries. *ACS applied materials & interfaces*, *6*(21), 19360-19370. https://doi.org/10.1021/am505448a

[46] **Adegbola, T. A., Agboola, O., & Fayomi, O. S. I.** (2020). Review of polyacrylonitrile blends and application in manufacturing technology: recycling and environmental impact. *Results in Engineering*, *7*, 100144. https://doi.org/10.1016/j.rineng.2020.100144

[47] **Dirican, M., Yan, C., Zhu, P., & Zhang, X.** (2019). Composite solid electrolytes for all-solid-state lithium batteries. *Materials Science and Engineering: R: Reports*, *136*, 27-46. https://doi.org/10.1016/j.mser.2018.10.004

[48] **Li, Y., Wang, J., Tang, J., Liu, Y., & He, Y.** (2009). Conductive performances of solid polymer electrolyte films based on PVB/LiClO4 plasticized by PEG200, PEG400 and PEG600. *Journal of Power Sources*, *187*(2), 305-311. https://doi.org/10.1016/j.jpowsour.2008.11.126

[49] **Klongkan, S., & Pumchusak, J.** (2015). Effects of nano alumina and plasticizers on morphology, ionic conductivity, thermal and mechanical properties of PEO-LiCF3SO3 solid polymer electrolyte. *Electrochimica Acta*, *161*, 171-176. https://doi.org/10.1016/j.electacta.2015.02.074

[50] **Url-2** https://www.sigmaaldrich.com/TR/en/search/polyethylene-glycol-1500?focus=products&page=1&perpage=30&sort=relevance&term=polyethylene%20glycol%201500&type=product/>, date retrieved 15.10.2023.

[51] **Huang, C. W., Wu, C. A., Hou, S. S., Kuo, P. L., Hsieh, C. T., & Teng, H.** (2012). Gel electrolyte derived from poly (ethylene glycol) blending poly (acrylonitrile) applicable to roll-to-roll assembly of electric double layer capacitors. *Advanced Functional Materials*, *22*(22), 4677-4685. https://doi.org/10.1002/adfm.201201342

[52] **Jung, H. R., Ju, D. H., Lee, W. J., Zhang, X., & Kotek, R.** (2009). Electrospun hydrophilic fumed silica/polyacrylonitrile nanofiber-based composite electrolyte membranes. *Electrochimica Acta*, *54*(13), 3630-3637. https://doi.org/10.1016/j.electacta.2009.01.039

[53] **Ramesh, S., & Wen, L. C.** (2010). Investigation on the effects of addition of SiO 2 nanoparticles on ionic conductivity, FTIR, and thermal properties of nanocomposite PMMA–LiCF3SO3–SiO2. *Ionics*, *16*, 255-262. https://doi.org/10.1007/s11581-009-0388-3

[54] **Wang, Y., Chen, M., Xie, Y., Wei, P., Schaefer III, H. F., Schleyer, P. V. R., & Robinson, G. H.** (2015). Stabilization of elusive silicon oxides. *Nature chemistry*, *7*(6), 509-513. https://doi.org/10.1038/nchem.2234

[55] **Armand, M., Axmann, P., Bresser, D., Copley, M., Edström, K., Ekberg, C., ... & Zhang, H.** (2020). Lithium-ion batteries–Current state of the art and anticipated developments. *Journal of Power Sources*, *479*, 228708. https://doi.org/10.1016/j.jpowsour.2020.228708

[56] **Marcinek, M., Syzdek, J., Marczewski, M., Piszcz, M., Niedzicki, L., Kalita, M., ... & Wieczorek, W.** (2015). Electrolytes for Li-ion transport–Review. *Solid State Ionics*, *276*, 107-126. https://doi.org/10.1016/j.ssi.2015.02.006

[57] **Park J. K.** (2012). Electrolytes. In *Principles and Applications of Lithium Secondary Batteries* (pp. 141–194). https://doi.org/10.1002/9783527650408.ch5

[58] **Min, H. S., Ko, J. M., & Kim, D. W.** (2003). Preparation and characterization of porous polyacrylonitrile membranes for lithium-ion polymer batteries. *Journal of power sources*, *119*, 469-472. https://doi.org/10.1016/S0378-7753(03)00206-4

[59] **Baskoro, F., Wong, H. Q., & Yen, H. J.** (2019). Strategic structural design of a gel polymer electrolyte toward a high efficiency lithium-ion battery. *ACS Applied Energy Materials*, *2*(6), 3937-3971. https://doi.org/10.1021/acsaem.9b00295

[60] **Smith, B. C.** (2011). *Fundamentals of Fourier transform infrared spectroscopy* (2nd ed.). CRC Press. https://doi.org/10.1201/b10777

[61] **Arya, A., & Sharma, A. L.** (2017). Polymer electrolytes for lithium ion batteries: a critical study. *Ionics*, *23*(3), 497-540. https://doi.org/10.1007/s11581-016-1908-6

[62] **Yap, Y. L., You, A. H., Teo, L. L., & Hanapei, H. J. I. J. E. S.** (2013). Inorganic filler sizes effect on ionic conductivity in polyethylene oxide (PEO) composite polymer electrolyte. *International Journal of Electrochemical Science*, *8*(2), 2154-2163. https://doi.org/10.1016/S1452-3981(23)14298-2

[63] **Nandiyanto, A. B. D., Oktiani, R., & Ragadhita, R.** (2019). How to read and interpret FTIR spectroscope of organic material. *Indonesian Journal of Science and Technology*, *4*(1), 97-118. https://doi.org/10.17509/ijost.v4i1.15806

[64] **KHAN, W. S.** (2017). Chemical and thermal investigations of electrospun polyacrylonitrile nanofibers incorporated with various nanoscale inclusions. *Journal of Thermal Engineering*, *3*(4), 1375-1390. https://doi.org/10.18186/journal-of-thermal-engineering.330180

[65] **Deivanayagam, R., & Shahbazian-Yassar, R.** (2021). Electrochemical methods and protocols for characterization of ceramic and polymer electrolytes for rechargeable batteries. *Batteries & Supercaps*, *4*(4), 596-606. https://doi.org/10.1002/batt.202000221

[66] **Abdul Halim, S. I., Chan, C. H., & Apotheker, J.** (2021). Basics of teaching electrochemical impedance spectroscopy of electrolytes for ion-rechargeable batteries–part 1: a good practice on estimation of bulk resistance of solid polymer electrolytes. *Chemistry Teacher International*, *3*(2), 105-115. https://doi.org/10.1515/cti-2020-0011

[67] **Muchakayala, R., Song, S., Gao, S., Wang, X., & Fan, Y.** (2017). Structure and ion transport in an ethylene carbonate-modified biodegradable gel polymer electrolyte. *Polymer Testing*, *58*, 116-125. https://doi.org/10.1016/j.polymertesting.2016.12.014

[68] **Flora, X. H., Ulaganathan, M., Babu, R. S., & Rajendran, S.** (2012). Evaluation of lithium ion conduction in PAN/PMMA-based polymer blend electrolytes for Li-ion battery applications. *Ionics*, *18*, 731-736. https://doi.org/10.1007/s11581-012-0690-3

[69] **Aziz, S. B., Woo, T. J., Kadir, M. F. Z., & Ahmed, H. M.** (2018). A conceptual review on polymer electrolytes and ion transport models. *Journal of Science: Advanced Materials and Devices*, *3*(1), 1-17. https://doi.org/10.1016/j.jsamd.2018.01.002

[70] **Choi, W., Shin, H. C., Kim, J. M., Choi, J. Y., & Yoon, W. S.** (2020). Modeling and applications of electrochemical impedance spectroscopy (EIS) for lithium-ion batteries. *Journal of Electrochemical Science and Technology*, *11*(1), 1-13. https://doi.org/10.33961/jecst.2019.00528

[71] **Du, Z., Su, Y., Qu, Y., Zhao, L., Jia, X., Mo, Y., ... & Chen, Y.** (2019). A mechanically robust, biodegradable and high performance cellulose gel membrane as gel polymer electrolyte of lithium-ion battery. *Electrochimica acta*, *299*, 19-26. https://doi.org/10.1016/j.electacta.2018.12.173

[72] **Zhang, X., Zhao, S., Fan, W., Wang, J., & Li, C.** (2019). Long cycling, thermal stable, dendrites free gel polymer electrolyte for flexible lithium metal batteries. *Electrochimica Acta*, *301*, 304-311. https://doi.org/10.1016/j.electacta.2019.01.156

[73] **Ding, C., Fu, X., Li, H., Yang, J., Lan, J. L., Yu, Y., ... & Yang, X.** (2019). An ultrarobust composite gel electrolyte stabilizing ion deposition for long-life lithium metal batteries. *Advanced Functional Materials*, *29*(43), 1904547. https://doi.org/10.1002/adfm.201904547

[74] **Pal, P., & Ghosh, A.** (2018). Influence of TiO2 nano-particles on charge carrier transport and cell performance of PMMA-LiClO4 based nano-composite electrolytes. *Electrochimica Acta*, *260*, 157-167. https://doi.org/10.1016/j.electacta.2017.11.070

[75] **Karbownik, I., Rac-Rumijowska, O., Fiedot-Toboła, M., Rybicki, T., & Teterycz, H.** (2019). The preparation and characterization of polyacrylonitrile-polyaniline (PAN/PANI) fibers. *Materials*, *12*(4), 664. https://doi.org/10.3390/ma12040664

[76] **Marcos, M. A., Cabaleiro, D., Guimarey, M. J., Comuñas, M. J., Fedele, L., Fernández, J., & Lugo, L.** (2017). PEG 400-based phase change materials nano-enhanced with functionalized graphene nanoplatelets. *Nanomaterials*, *8*(1), 16. https://doi.org/10.3390/nano8010016

[77] **Pramono, E., Utomo, S. B., Wulandari, V., & Clegg, F.** (2016). FTIR studies on the effect of concentration of polyethylene glycol on polimerization of Shellac. In *Journal of Physics: Conference Series* (Vol. 776, No. 1, p. 012053). IOP Publishing. https://doi.org/10.1088/1742-6596/776/1/012053

[78] **Shameli, K., Ahmad, M. B., Jazayeri, S. D., Sedaghat, S., Shabanzadeh, P., Jahangirian, H., ... & Abdollahi, Y.** (2012). Synthesis and characterization of polyethylene glycol mediated silver nanoparticles by the green method. *International journal of molecular sciences*, *13*(6), 6639-6650. https://doi.org/10.3390/ijms13066639

[79] **Liu, X., Wang, C., Cai, Z., Hu, Z., & Zhu, P.** (2022). Fabrication and characterization of polyacrylonitrile and polyethylene glycol composite nanofibers by electrospinning. *Journal of Energy Storage*, *53*, 105171. https://doi.org/10.1016/j.est.2022.105171

[80] **Ke, G., & Jin, X.** (2021). Fabrication and characterizations of electrospun PAN/PEG1000/2000 composite fibres. *Indian Journal of Fibre & Textile Research (IJFTR)*, *46*(1), 34-40. https://doi.org/10.56042/ijftr.v46i1.24870

[81] **Wu, Y., Liu, Z., & Ran, F.** (2019). New comprehensions on structure superiority of asymmetric carbon membrane and controlled construction of advanced hierarchical inner-structure for high performance supercapacitors. *Microporous and Mesoporous Materials*, *275*, 14-25. https://doi.org/10.1016/j.micromeso.2018.08.011

[82] **Danquah, S. A., Strimaitis, J., Denize, C. F., Pradhan, S. K., & Bahoura, M.** (2022). LLCZN/PEO/LiPF6 composite solid-state electrolyte for safe energy storage application. *Batteries*, *8*(1), 3. https://doi.org/10.3390/batteries8010003

[83] **Furushima, Y., Nakada, M., Takahashi, H., & Ishikiriyama, K.** (2014). Study of melting and crystallization behavior of polyacrylonitrile using ultrafast differential scanning calorimetry. *Polymer*, *55*(13), 3075-3081. https://doi.org/10.1016/j.polymer.2014.05.015

[84] **Kou, Y., Wang, S., Luo, J., Sun, K., Zhang, J., Tan, Z., & Shi, Q.** (2019). Thermal analysis and heat capacity study of polyethylene glycol (PEG) phase change materials for thermal energy storage applications. *The Journal of Chemical Thermodynamics*, *128*, 259-274. https://doi.org/10.1016/j.jct.2018.08.031

[85] **Lin, D., Liu, W., Liu, Y., Lee, H. R., Hsu, P. C., Liu, K., & Cui, Y.** (2016). High ionic conductivity of composite solid polymer electrolyte via in situ synthesis of monodispersed SiO2 nanospheres in poly (ethylene oxide). *Nano letters*, *16*(1), 459-465. https://doi.org/10.1021/acs.nanolett.5b04117

[86] **Sharma, R., Sil, A., & Ray, S.** (2016). Poly (methyl methacrylate) based nanocomposite gel polymer electrolytes with enhanced safety and performance. *Journal of Polymer Research*, *23*, 1-8. https://doi.org/10.1007/s10965-016-1049-7

[87] **Hadad, S., Hamrahjoo, M., Dehghani, E., Salami-Kalajahi, M., Eliseeva, S. N., Moghaddam, A. R., & Roghani-Mamaqani, H.** (2022). Cellulose-based solid and gel polymer electrolytes with super high ionic conductivity and charge capacity for high performance lithium ion batteries. *Sustainable Materials and Technologies*, *33*, e00503. https://doi.org/10.1016/j.susmat.2022.e00503

CURRICULUM VITAE

Name Surname **:** Sabiha Ezgi KAYA

EDUCATION **:**

- **B.Sc.** **:** 2017, Istanbul Technical University, Faculty of Chemical and Metallurgical Engineering, Department of Chemical Engineering

PUBLICATIONS, PRESENTATIONS AND PATENTS ON THE THESIS:

- Karatepe N. and **Kaya S.E.** 2023: Thermal and Electrochemical Properties of a Polyacrylonitrile-based Lithium-Ion Conducting Quasi-Solid-State Electrolyte. 2nd International Graduate Research Symposium – IGRS'23, May 16-18, 2023 Istanbul, Turkey.